Available online at www.CivileJournal.org

Civil Engineering Journal

(E-ISSN: 2476-3055; ISSN: 2676-6957)

Vol. 10, No. 11, November, 2024

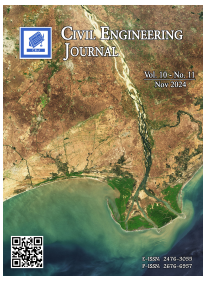

Analyzing the Future Climate Change Impacts on Meteorological Parameters Using the LARS-WG Model

Mohammed A. Dheyaa [1*], Mustafa M. Al-Mukhtar [1], Khalid Shemal [2]

[1] *Department of Civil Engineering, University of Technology, Baghdad, Iraq.*

[2] *The General Commission for Irrigation and Reclamation Projects, Iraqi Ministry of Water Resources, Baghdad, Iraq.*

Received 15 July 2024; Revised 22 September 2024; Accepted 09 October 2024; Published 01 November 2024

Abstract

This research aims to evaluate the impacts of climate changes and reveal the future trends on meteorological parameters, i.e., precipitation and temperature effects, in three major cities in Iraq, namely Baghdad, Wasit, and Maysan, which are located along the Tigris River basin. The LARS-WG8.0 model was employed, and five GCMs were used within CMIP6 under three different scenarios, i.e., SSP126, SSP245, and SSP585, for the period 2021-2100. The observed and simulated data were tested by the statistical criteria R, R^2, NSE, and RMSE through the baseline period 2003-2022. In addition, using the K-S test for validation of the LARS-WG8.0 model resulted in accuracy and reliability. The future projections indicate that the average temperatures will increase until the end of the current century, with a difference of 1.86, 2.85, and 5.36°C. The fluctuations in precipitation occur throughout the winter, spring, and autumn months. The highest precipitation was recorded in December and January. Therefore, all GCMs give a unified indicator of future climate forecasts. Rising temperatures and fluctuations in precipitation negatively impacted water and food security. As a result, this will impact the water resources and agricultural sectors. This research contributes to exploring the future climate behavior of the study area.

Keywords: LARS-WG; GCMs; SSPs; Tigris River; Precipitation; Temperatures; Climate Change.

1. Introduction

Climate change is a global concern with far-reaching ramifications in terms of its impact on the ecological and hydrological systems [1], as well as social and economic aspects, such as its impact on water and food security represented by the sectors of water resources and agriculture [2, 3]. Moreover, climate change behavior is interpreted based on a comprehensive analysis of previous climate data through projected precipitation patterns and temperatures [4]. Human activities, including the utilization of fossil fuels, deforestation, and industrial processes that generate greenhouse gases into the atmosphere, are mostly to blame. These gases trap heat from the sun, causing global temperatures to rise and shifting weather patterns across the earth, according to IPCC-AR6 2022. In its AR6 report, the IPCC assessed projected temperature outcomes for a set of five-stage scenarios under the CMIP framework; these scenarios are named SSPs (SSP1–SSP5) based on the anticipated range of radiative effect in 2100 (1.9–8.5 W/m^2) [5, 6]. The CMIP is a collaborative effort framework designed to facilitate the development of GCMs, which provide climate projections globally, allowing policymakers to develop more effective strategies for managing the impacts of global warming depending on the information presented [7].

The Middle East is recognized as the most impacted portion of the world by global climate change during the past few years due to an arid and semi-arid nature [8, 9]. Therefore, decreased precipitation combined with rising

* Corresponding author: bce.22.12@grad.uotechnology.edu.iq

http://dx.doi.org/10.28991/CEJ-2024-010-11-019

temperatures will eventually lead to water scarcity and increased drought [10]. As a result, it is expected that the region will face environmental problems such as reduced water availability, extreme heat waves, flash floods, and frequent dust storms [11]. The extreme increase in climate phenomena leads to environmental deterioration in most parts of the country, which makes it necessary to evaluate the impact of climate and hydrological changes on water availability. This is what was presented by the latest studies, which concluded that the observed climate phenomena tend to increase due to climate change in the countries of the Middle East [12–15]. Therefore, understanding the consequences of climate change requires the use of software techniques and methods; one of these methods is the use of weather generator models, which are computerization and statistical models that simulate weather conditions based on recorded meteorological data to fill in missing values and create a synthetic series of data [16, 17]. Thus, weather generators are important in studying climate change and its impacts on several sectors, such as hydrology, agriculture, energy, and urban planning. GCMs provide data with limited spatial resolution; hence, they cannot be directly used to evaluate the influences of climate change. However, to improve the spatial accuracy of the data, downscaling techniques must be applied [18, 19]. There are several random weather generators specialized in the field of future and current climate predictions; one of these generators is the LARS-WG model issued by "Long Ashton Research Station". The LARS-WG model is widely used for climate projections and downscaling of present and future climate data [20]. It was developed specifically to assess the consequences of climatic changes and tested under different conditions, where it showed its superiority over other weather generators.

In the literature, there are many successful applications of LARS-WG in different locations of the world [20–22] considering various GCMs [23–25]. Semenov et al. [26] evaluated the LARS-WG8.0 weather generator in the study area of Great Britain (England, Scotland, and Wales) using observed climate data from 85 meteorological stations of the period 1985-2015 to generate projected future data of precipitation and temperatures for the periods 2021-2040 and 2041-2060. Five GCMs from the CMIP6 report were used, namely ACCESS-ESM1-5, CNRM-CM6-1, HadGEM3-GC31-LL, MPI-ESM1-2-LR, and MRI-ESM2-0. It was demonstrated that the LARS-WG model effectively forecasts future climate fluctuations and extreme events. Shahi et al. [27] studied the impact of climate change on meteorological variables and surface water in a study area located in the Iranian Semnan Province to manage flood control and store excess water in non-agricultural seasons. They predicted future precipitation and temperatures using the LARS-WG model during the period 2002-2020. Two different GCMs, namely CaneSM5 and HadGem3, were used under three different scenarios, namely SSP126, SSP245, and SSP585, to generate future data for the period 2020-2040. They noticed that there was inherent uncertainty among the imposed climate scenarios due to the complexity of the climate systems, which was attributed to the difference between future conditions and the selected study period. However, they recommended intensifying future studies and providing more detailed predictions to mitigate the effects of climate change.

Nouri et al. [28] assessed the environmental and hydrological impact of climate change in two regions, Taham and Golabar, within Zanjan Province. The climate variables for the future periods 2020-2030 and 2046-2065 were predicted based on historical data through the application of the LARS-WG. They used three different GCMs, namely HADCM3, CSIROMK3, and IPSLCM4, under two different scenarios, namely A1B and B1. The LARS-WG model demonstrated its ability and effectiveness in producing forecast results that are more accurate and reliable in terms of downscaled outputs and statistical representation. They found that the uncertainty in the scenarios used is relatively low for temperature forecasts but higher for precipitation because of its fluctuations in future projections.

Muheisen et al. [29] used the LARS-WG6.0 in the Mosul Dam watershed to study future trends in temperature and precipitation projections during the future periods by applying four GCMs, namely BCC-CSM1-1, CSIRO_MK3.6, HaDGEM2-ES, and NorESM1-M, under three different scenarios, namely RCP2.6, RCP4.5, and RCP8.5. They revealed an increase in temperature rates of 1.3, 2.4, and 4.5 °C, as well as a decrease in the simulated average annual precipitation to 772, 756.7, and 741.6 mm/year at the end of the current century under the RCP2.6, RCP4.5, and RCP8.5 scenarios, respectively. Al-Hasani et al. [30] studied the impact of long-term climate change in Kirkuk Governorate in Iraq by predicting precipitation during the future period using the LARS-WG7.0 model. They used five different GCMs, namely CSIRO-Mk3.6.0, HadGEM2-ES, CanESM2, MIROC5, and NorESM1-M, to analyze water scarcity due to climate change in arid and semi-arid regions. They found that there was a decrease in precipitation, which led to a significant reduction in surface runoff flow.

Saeed et al. [31] employed LARS-WG6.0 in the Diyala River basin shared between Iraq and Iran to evaluate the hydrological response under the influence of climate change during the future periods 2021-2040, 2041-2060, and 2061-2080, under three different scenarios, namely RCP2.6. , RCP4.5, and RCP8.5, and five GCMs, namely BCC-CSM1, CanESM2, CSIRO-MK36, HadGEM2-ES, and NorESM1. The study addressed future trends in climate variables during the future period, which contributed to providing insights into how climate change will impact water availability in basins located within arid and semi-arid regions. They revealed that the basin will experience a temperature rise of 6.6, 10.1, and 16.6% for scenarios RCP2.6, RCP4.5, and RCP8.5, respectively. Furthermore, precipitation will probably decrease by 3.2, 6.4, and 8.7%, leading to a 38.8, 47.9, and 52.8% decrease in streamflow under scenarios RCP2.6, RCP4.5, and RCP8.5, in the order given.

In this study, the effects of future climate changes on precipitation and temperature data for three meteorological sites representing central and southern Iraq, located on the Tigris River basin, namely Baghdad, Wasit, and Maysan, were identified. The LARS-WG8.0 model was employed to downscale five GCMs data, i.e., ACCESS-ESM1-5, CNRM-CM6-1, HadGEM3-GC31-LL, MPI-ESM1-2-LR, and MRI-ESM2-0, under three different scenarios, SSP126, SSP245, and SSP585. The future trends of the meteorological parameters were analyzed over four future periods, i.e., 2021-2040, 2041-2060, 2061-2080, and 2081-2100. The findings of this study could be used to introduce a better plan for water management in the study area.

2. Research Methodology

2.1. Description of Study Area Data

Iraq is a Middle Eastern country with a total area of 437,072 km² and is located in an area with consistent climate fluctuations. Its lands are occasionally exposed to aridity and drought, which negatively impact water resources and agriculture. Therefore, it is important to investigate its vulnerability to the negative consequences of climate changes. This study includes three meteorological stations located in three governorates along the Tigris River basin, namely Baghdad, Wasit, and Maysan, as shown in Figure 1. Table 1 provides information on the locations of the three meteorological stations.

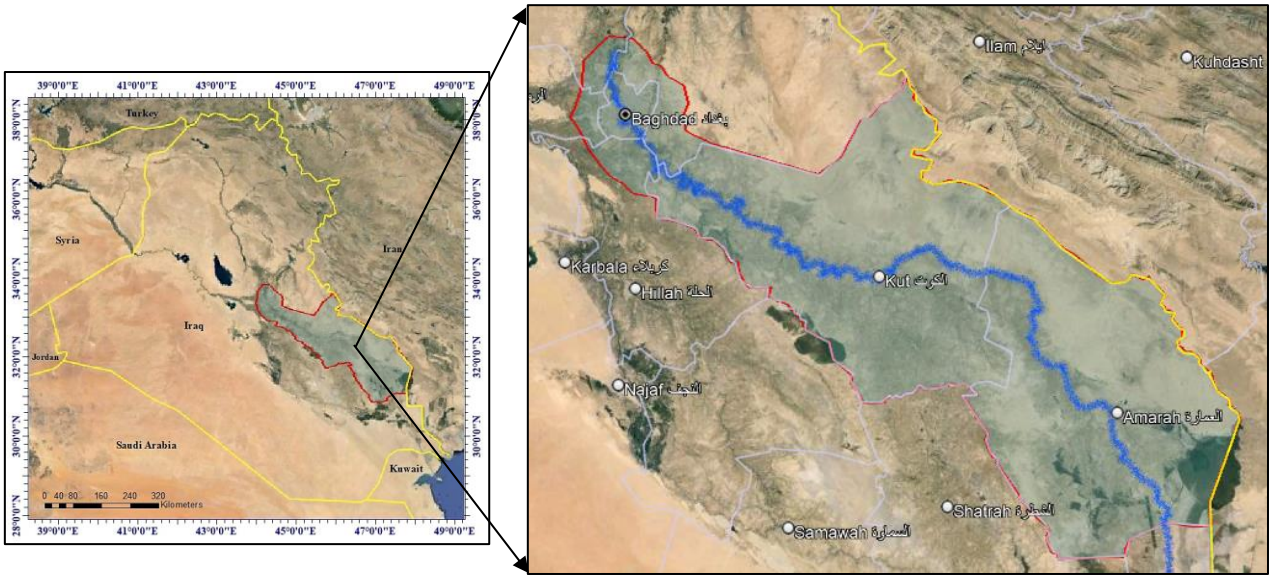

Figure 1. A map showing the study area

Table 1. Location details of the three meteorological stations in three governorates in Iraq

Location	Latitude	Longitude	Altitude
Baghdad	33°18´ N	44°24´ E	31.7 m
Wasit	32°3´ N	45°49´ E	19 m
Maysan	31°5´ N	47°1´ E	9.5 m

The data collected includes daily precipitation, solar radiation, and MAX/MIN temperatures at the studied stations. The source of this data was NASA satellite observations *(https://power.larc.nasa.gov)* with a resolution of 0.5x0.5 degrees per grid and CHIRPS ***(****https://app.climateengine.org/climateEngine****)*** with a high resolution of 0.05x0.05 degrees per grid. The period 2003-2022 was adopted as a baseline period and used to validate the model. The satellite data were initially validated against counterpart data from ground stations.

2.2. LARS-WG Model Description

LARS-WG is a stochastic weather generator that is an effective tool for downscaling daily climate data generated to assess climate changes based on GCMs estimates. It has been used in many regions for studies and research, where it has been extensively verified in a variety of regions throughout the world [31]. The LARS-WG simulation requires four weather variables: maximum temperature (T_{max}), minimum temperature (T_{min}), solar radiation, and precipitation. Using a complicated statistical distribution model, it produces daily time series data that are statistically comparable to actual data that was observed. LARS-WG's modeling depends on the length of dry and wet periods, so it evaluates recorded weather based on characteristics of statistics and generates a site-specific accumulated probability of wet and dry series

distributions for various meteorological variables such as daily MIN and MAX temperature and precipitation. Through LARS-WG, better results and estimates of site parameters are obtained when using observed data for at least 20-30 years, which is statistically sufficient to ensure that all climate events, including extreme events, are considered. This is considered extremely important to ensure the accuracy of the results. A semi-empirical distribution is employed in the LARS-WG model, which represents a more accurate distribution, and it is based on estimating the wet/dry sequences distributions of daily MAX/MIN temperatures and precipitation, where *Pi* and *Xi* represent probability and climate variables, respectively, as shown in the following formula:

$$Xi = min\ [\ X : P\ (X_{obs} \leq X) \geq Pi\ ]\ i = 0, \ldots, n, \quad (1)$$

$$X_0 = min\{\ X_{obs}\ \}, \quad (2)$$

$$X_n = max\{\ X_{obs}\ \}. \quad (3)$$

The probability *P* depends entirely on the observed variables X_{obs}, where its values range from 0 to 1. One of the advantages of the LARS-WG model is that it accurately approximates variables with extreme values by specifying a set of probabilities *Pi* for low values that are close to zero and for high values that are close to one. The values of the remaining variables are distributed equally during the interval between the highest and lowest values of the observed data for the same month, according to the probability value *Pi* for each variable. The high probability value *P* for the occurrence of daily precipitation, whose value as a variable is relatively low, is less than 1 mm. Its impact on the model's outputs will be minimal. Therefore, it is calculated according to probabilities through $Pi = P\ (X_{obs} \leq Xi)$; i = 1, 2, and this indicates that the amount of precipitation is insufficient to exceed the observed value because it is less than 1 mm despite its high probability value *Pi*. It is being calculated using two values close to one for a very long wet and dry series. For example, the values P_{n-1} = 0.99 and P_{n-2} = 0.98 are used. As for calculating the MAX/MIN temperatures, they are limited to between 0 and 1 by choosing two values. close to zero and two values close to one; for instance, P_{n-1} = 0.99, P_{n-2} = 0.98, P_2 = 0.01, and P_3 = 0.02. That is, all probability values are P_i ($0 < i < 1$).

The LARS-WG8.0 version includes 15 GCMs representing climate projections from the latest CMIP6 ensemble utilized in the IPCC-AR6. The LARS-WG has several properties that make it appropriate for weather projections. Five different GCMs were used in this study, as shown in Table 2. Future climate data are predicted and evaluated according to the practical steps of the methodology used in this research, demonstrated in Figure 2.

Table 2. Selected five GCMs from IPCC-AR6 incorporated into the LARS-WG8.0 in this study

GCM	Center of Research	Location	Grid resolution (lat. x long.)
ACCESS-ESM1-5	Commonwealth Scientific and Industrial Research Organization (CSIRO)	Australia	1.25° × 1.875°
CNRM-CM6-1	Centre National de Recherche's Methodologies (CNRM), Centre European de Recherche et de Formation Advance en Calcul Scientifique (CERFACS)	France	1.40° × 1.406°
HadGEM3-GC31-LL	UK Met Office Hadley Centre (MOHC)	UK	1.25° × 1.88°
MPI-ESM1-2-LR	Max Planck Institute for Meteorology (MPI-M)	Germany	1.39° × 1.41°
MRI-ESM2-0	Meteorological Research Institute (MRI)	Japan	1.113° × 1.125°

2.3. LARS-WG Model Performance Indices

A set of statistical assessment tests was employed in this study to conduct the calibration and validation of the model, where the K-S test was adopted as a statistical test to verify the seasonal distributions, such as the correspondence of the wet/dry series, as well as the distributions of daily temperatures and precipitation. Through the K-S test, indicators of acceptance and rejection can be obtained using the P-value of 0.05, which shows that the hypothesis between the distributions is identical or vice versa [32–34], as shown in Table 3.

Table 3. Lists the acceptable limits of K-S test values used in evaluating the LARS-WG outcomes

Range	Classification
P-value = 1	Perfect
0.7 < P-value < 1	Very good
0.4 < P-value < 0.7	Good
0.4 > P-value	Poor

Sometimes, differences in results may appear between the observed and generated data due to several factors, including errors in transmitting the observed data and random variation occurring in the data. In addition to abnormal climate events observed at one of the stations, which may classify that point as anomalous due to its deviation from the

rest of the observed points. This is known as extreme weather, which will negatively impact the data accuracy during its verification. Therefore, other statistical indices were used to demonstrate the application performance. Four statistical standards were used, namely the correlation coefficient R (Equation 4), the determination coefficient R^2 (Equation 5), the Nash-Sutcliff efficiency coefficient NSE (Equation 6), and the root mean square error RMSE (Equation 7).

$$R = \frac{\Sigma[Ai - Aav][Bi - Bav]}{\sqrt{\Sigma(Ai - Aav)^2 \, \Sigma(Bi - Bav)^2}} \quad (4)$$

$$R^2 = \frac{(\Sigma[Ai - Aav][Bi - Bav])^2}{\Sigma(Ai - Aav)^2 \, \Sigma(Bi - Bav)^2} \quad (5)$$

$$NSE = 1 - \frac{\sum_{i=1}^{m}(Ai - Bi)^2}{\sum_{i=1}^{m}(Ai - Bav)^2} \quad (6)$$

$$RMSE = \sqrt{\frac{\sum_{i=1}^{m}(Ai - Bi)^2}{m}} \quad (7)$$

where A_i is observed value, A_{av} is average observed value, B_i is simulated value, B_{av} is average simulated value, and m is number of values. R, R^2, and NSE give the best result when they are closer to 1, while the lowest value of $RMSE$ indicates accurate model results and vice versa.

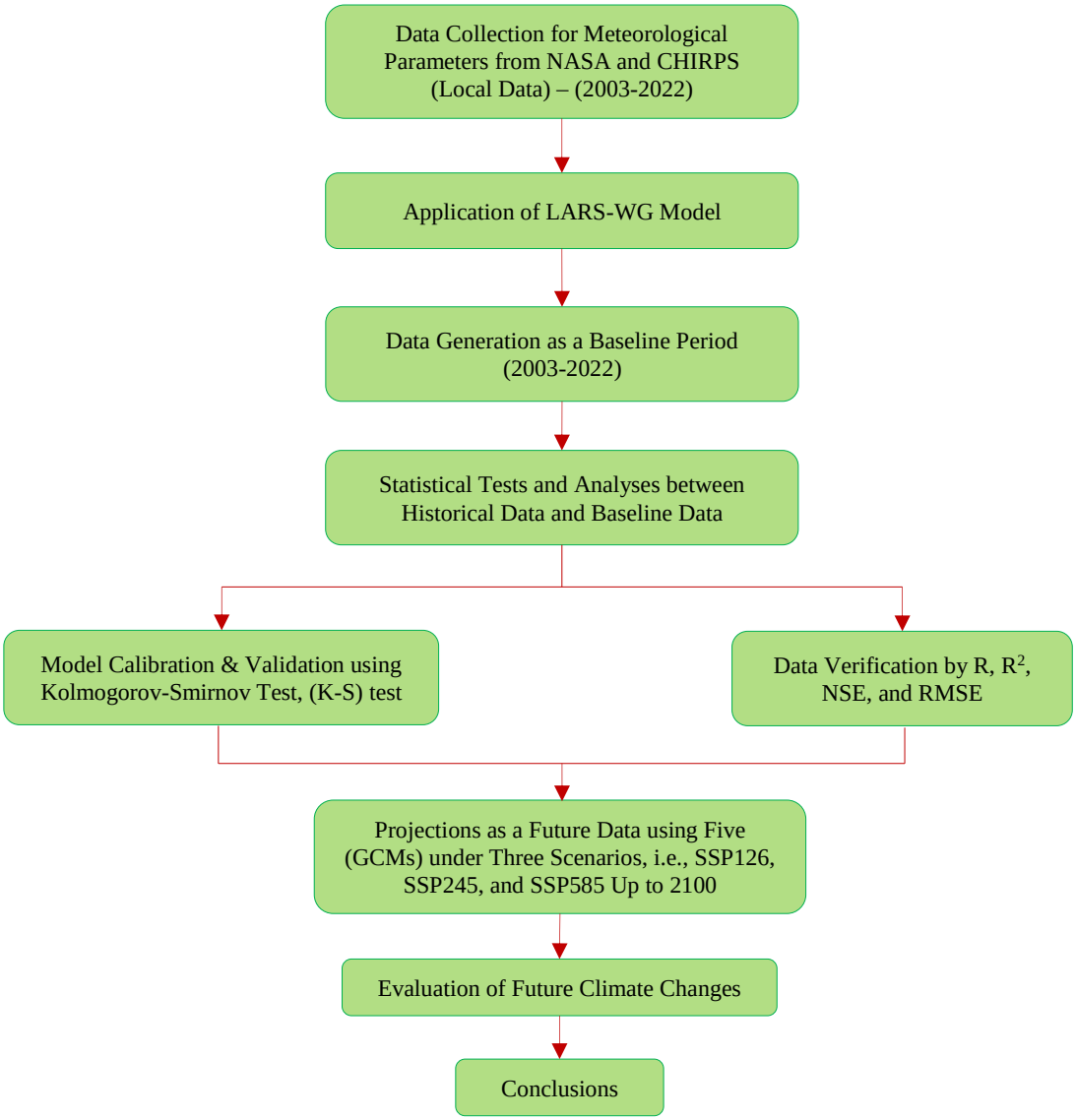

Figure 2. Flow chart of research methodology

3. Results and Discussion

3.1. LARS-WG Model Calibration and Validation Results

Validating the performance of the LARS-WG model is extremely important to identify the accuracy of its results. In this study, the K-S test was utilized to compare the seasonal distributions of the wet/dry series between the observed

and simulated values. Table 4 displays the statistical analysis findings of observed seasonal data for the selected meteorological stations. Table 5 presents the K-S test results for average monthly precipitation distributions. The P-value is evaluated according to the criteria set out in Table 3.

Table 4. The values of the (K-S) test for seasonal distributions of wet/dry series

Season	(K-S) test	P-value	N	Wet / Dry	Assessment
Baghdad station					
DJF	0.041	1	12	wet	Perfect
	0.089	1	12	dry	Perfect
MAM	0.015	1	12	wet	Perfect
	0.094	1	12	dry	Perfect
JJA	0.044	1	12	wet	Perfect
	0.391	0.043	12	dry	Poor
SON	0.092	1	12	wet	Perfect
	0.136	0.974	12	dry	Very good
Wasit station					
DJF	0.058	1	12	wet	Perfect
	0.106	0.999	12	dry	Very good
MAM	0.054	1	12	wet	Perfect
	0.138	0.971	12	dry	Very good
JJA	0	1	12	wet	Perfect
	0.348	0.096	12	dry	Poor
SON	0.051	1	12	wet	Perfect
	0.242	0.454	12	dry	Good
Maysan station					
DJF	0.068	1	12	wet	Perfect
	0.083	1	12	dry	Perfect
MAM	0.063	1	12	wet	Perfect
	0.283	0.267	12	dry	Poor
JJA	0.131	0.982	12	wet	Very good
	0.435	0.017	12	dry	Poor
SON	0.044	1	12	wet	Perfect
	0.184	0.789	12	dry	Very good

Table 5. The values of the (K-S) test for daily precipitation distributions

Month	(K-S) test	P-value	N	Assessment
Baghdad station				
January	0.13	0.984	12	Very good
February	0.064	1	12	Perfect
March	0.188	0.767	12	Very good
April	0.151	0.937	12	Very good
May	0.235	0.492	12	Good
June	0.305	0.193	12	Poor
July	No Precipitation			
August	No Precipitation			
September	0.565	0.001	12	Poor
October	0.165	0.884	12	Very good
November	0.115	0.996	12	Very good
December	0.093	1	12	Perfect

Wasit station				
January	0.065	1	12	Perfect
February	0.065	1	12	Perfect
March	0.129	0.985	12	Very good
April	0.05	1	12	Perfect
May	0.03	1	12	Perfect
June	1	0	12	Poor
July		No Precipitation		
August	1	0	12	Poor
September	0.493	0.004	12	Poor
October	0.19	0.755	12	Very good
November	0.119	0.994	12	Very good
December	0.13	0.984	12	Very good
Maysan station				
January	0.13	0.984	12	Very good
February	0.065	1	12	Perfect
March	0.215	0.607	12	Good
April	0.07	1	12	Perfect
May	0.349	0.094	12	Poor
June	0.131	0.982	12	Very good
July		No Precipitation		
August	1	0	12	Poor
September	0.477	0.007	12	Poor
October	0.206	0.661	12	Good
November	0.119	0.994	12	Very good
December	0.207	0.655	12	Good

The evaluation results shown in Tables 4 and 5 indicate that the performance of the LARS-WG model for simulating precipitation with seasonal and daily distributions is closer to the perfect fit in all seasons except in the summer. Especially those within the dry series distributions in which the precipitation rate is rather low. In Tables 4 and 5, it is clear that the model performs well in analyzing and interpreting the distribution of the wet / dry series. In the autumn seasons (SON) and winter (DJF), the evaluation ranges between very good and close to perfect. In contrast, in the spring season (MAM), the assessment varied between very good and perfect. In the summer season, (JJA) gives poor results in the dry series distributions due to the reduction of precipitation, which is considered a natural occurrence in Iraq, as there is no precipitation in the summer season. Figure 3 shows the observed versus simulated mean, standard deviation of precipitation, and temperatures across the three sites within the study area. It is noticeable that the model performed well in reproducing the standard deviation and mean of the evaluated parameters at all sites. As such, the LARS-WG8.0 model has proven its ability and efficiency in forecasting precipitation and MAX / MIN temperatures, suggesting its possibility to be applied as a weather generator model in arid and semi-arid regions.

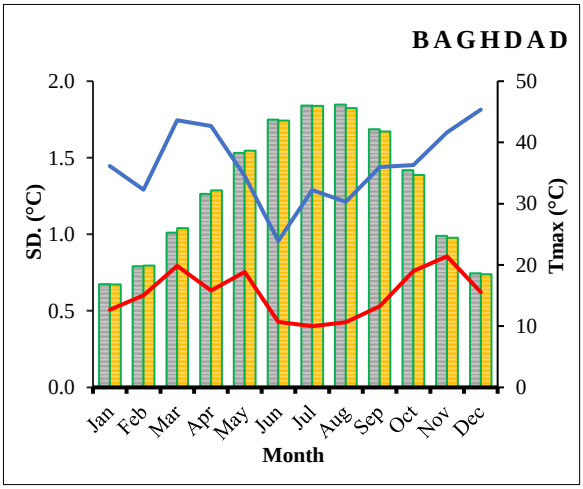

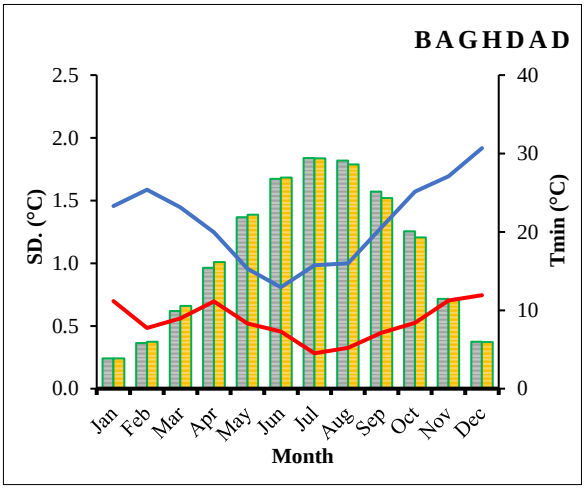

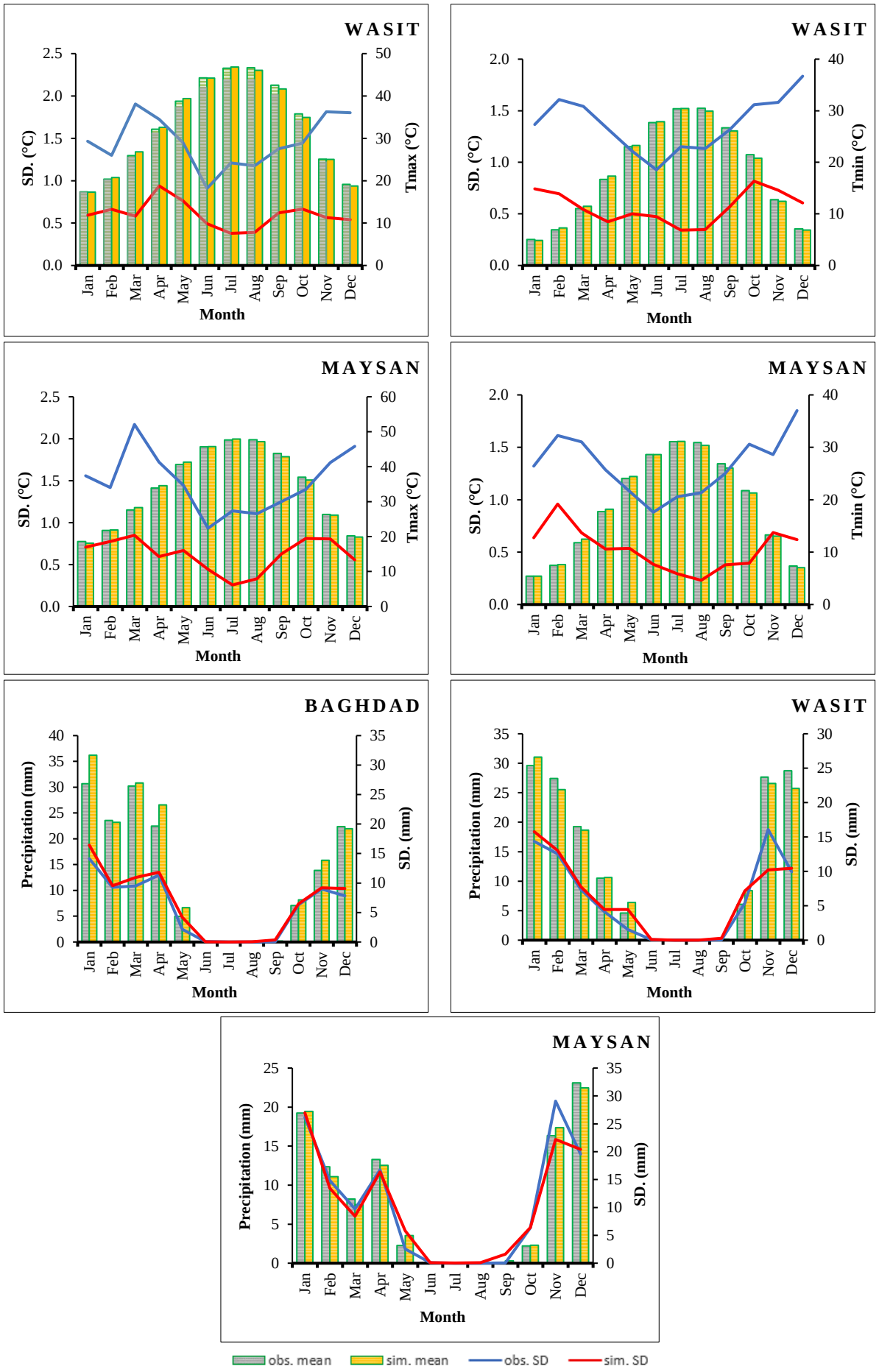

Figure 3. Comparison between observed and simulated monthly standard deviation and mean of MAX/MIN temperature and precipitation

Table 6 shows the statistical description of MAX/MIN temperatures and precipitation for the study area that was recorded over 20 years of the baseline (2003-2022). It is evident from the data recorded in the recent years of the historical period (base period) that the highest average monthly temperatures were recorded (in July), which exceeded 48 °C in the three locations. On the other side, the monthly precipitation rates were limited between the years 2018 and 2019 (in January and November), while the lowest average temperatures and the lowest precipitation rate were recorded in January during the year 2008. Therefore, it can be judged that the relationship between the two variables, temperature and precipitation, is very complex in the study area.

Table 6. Precipitation, and MAX / MIN temperatures recorded during the study period 2003-2022

Location	MAX value			MIN value		
	T_{max}	T_{min}	Rain	T_{max}	T_{min}	Rain
Baghdad	48.32	31.52	65.24	12.91	0.13	0
	Jul-2020	Jul-2021	Jan-2019	Jan-2008	Jan-2008	-
Wasit	48.93	32.50	81.84	13.37	1.85	0
	Jul-2017	Jul-2020	Nov-2018	Jan-2008	Jan-2008	-
Maysan	49.97	32.99	88.78	14.25	2.31	0
	Jul-2017	Jul-2020	Nov-2018	Jan-2008	Jan-2008	-

Table 7 shows the statistical indicators used between the observed and simulated parameters during the baseline period. Figure 4 depicts the error bar of the simulation results during the baseline. All results were satisfactory and within the limits of acceptance, which indicates the efficiency of the model to be used for future predictions.

Table 7. The statistical indicators used for verification of the LARS-WG model during 2003-2022

Station	Variable	R	R^2	NSE	RMSE
Baghdad	T_{max}	0.99	0.98	0.98	1.67
	T_{min}	0.99	0.97	0.97	1.56
	Precipitation	0.88	0.77	0.72	7.10
Wasit	T_{max}	0.99	0.98	0.98	1.68
	T_{min}	0.99	0.97	0.97	1.52
	Precipitation	0.76	0.58	0.52	9.79
Maysan	T_{max}	0.99	0.97	0.97	1.73
	T_{min}	0.84	0.71	0.67	5.30
	Precipitation	0.76	0.58	0.51	10.71

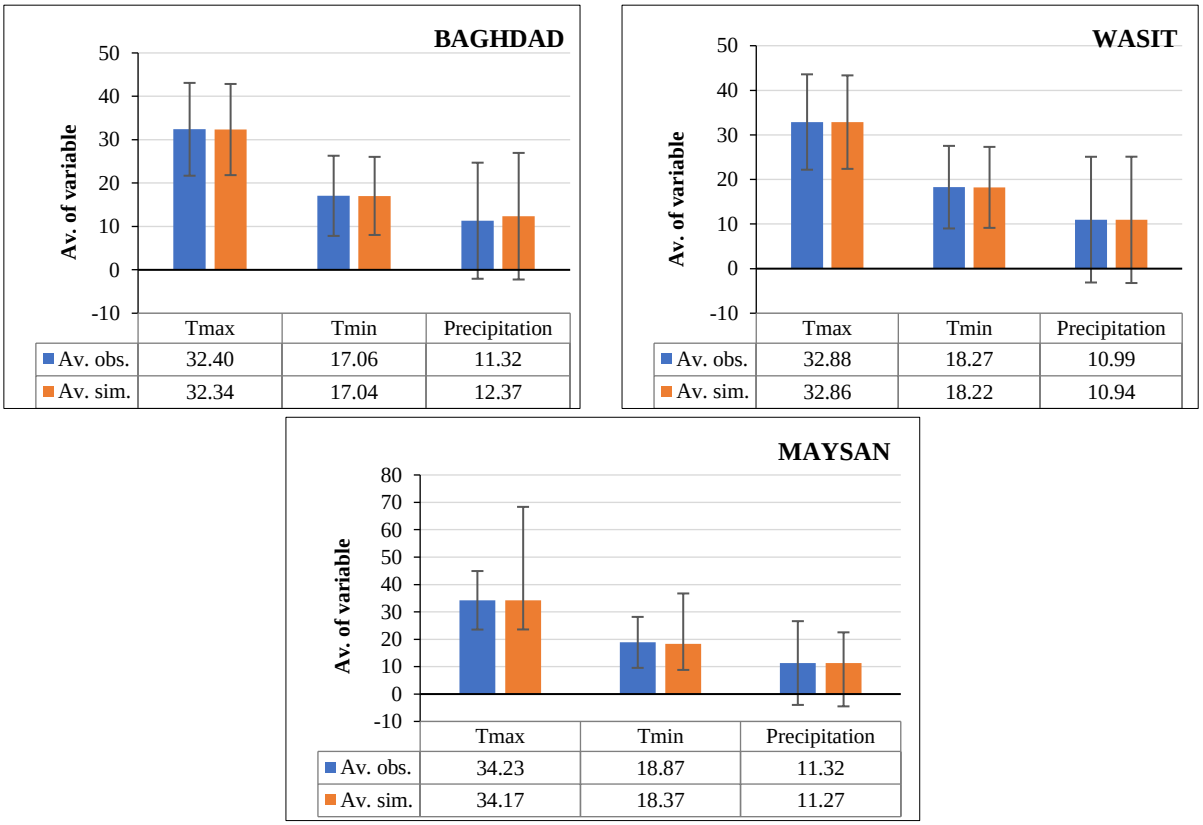

Figure 4. Error bar between simulated and observed MAX/MIN temperatures and precipitation

3.2. Temperature Projection in the Future

In this study, five different GCMs within CMIP6 are used for future climate projections under three different scenarios issued from the IPCC recommendations in their sixth report. The scenarios consist of the initial scenario, SSP126; the moderate scenario, SSP245; and the severe scenario, SSP585. The study area includes three Iraqi governorates located on the Tigris River basin, namely Baghdad, Wasit, and Maysan. The LARS-WG model was initially validated during the baseline before it was applied to project the future precipitation trend and temperatures. Figure 5 shows the future trend of annual mean MAX/MIN temperatures for all five GCMs under all three scenarios, SSP126, SSP245, and SSP585, for the entire study area. From the results, it is clear that future projections of the trend of MAX/MIN temperatures tend to rise gradually compared to the observed data until the end of the current century in 2100, where the annual average maximum temperatures during the period 2081-2100 are expected to reach 35.28, 36.27, and 38.78 °C under scenarios SSP126, SSP245, and SSP585, respectively. This implies that the expected increase in temperatures will be 1.86, 2.85, and 5.36 °C for the three scenarios, in the order given. Tables 8 and 9 show the highest and lowest values of the mean of MAX / MIN temperatures. The highest temperatures were recorded in the summer season in July and August, while the lowest value of MIN temperature was recorded in the winter season, especially in January.

It is noted that the forecasts for the lowest average minimum temperatures will be recorded in the near future, i.e., at the beginning of the future period, specifically in January in the year 2032 for all scenarios, while the forecasts for the highest average maximum temperatures in the distant future will be recorded in July of the year 2070 under scenario SSP126 and will be limited to July and August in the period 2070-2100. These results are consistent with those reported by Muheisen et al. [29, 35] and Saeed et al. [31]. Figure 6 shows average monthly temperatures during the future periods along with those of the baseline. It is noticeable that there is a continuous increase in the average projected MAX/MIN temperatures for the five GCMs during future periods. Suggesting that the study area is highly vulnerable to the impacts of climate change, which in turn might influence the water resources sector and agricultural activities in the region. Figure 7 shows the relative differences and the percentage increase in the annual average of MAX/MIN temperatures compared to the observed period. Undoubtedly, it is noticed that the entire area witnesses a positive relative difference, viz., there is an upward trend in the future temperatures concerning the baseline.

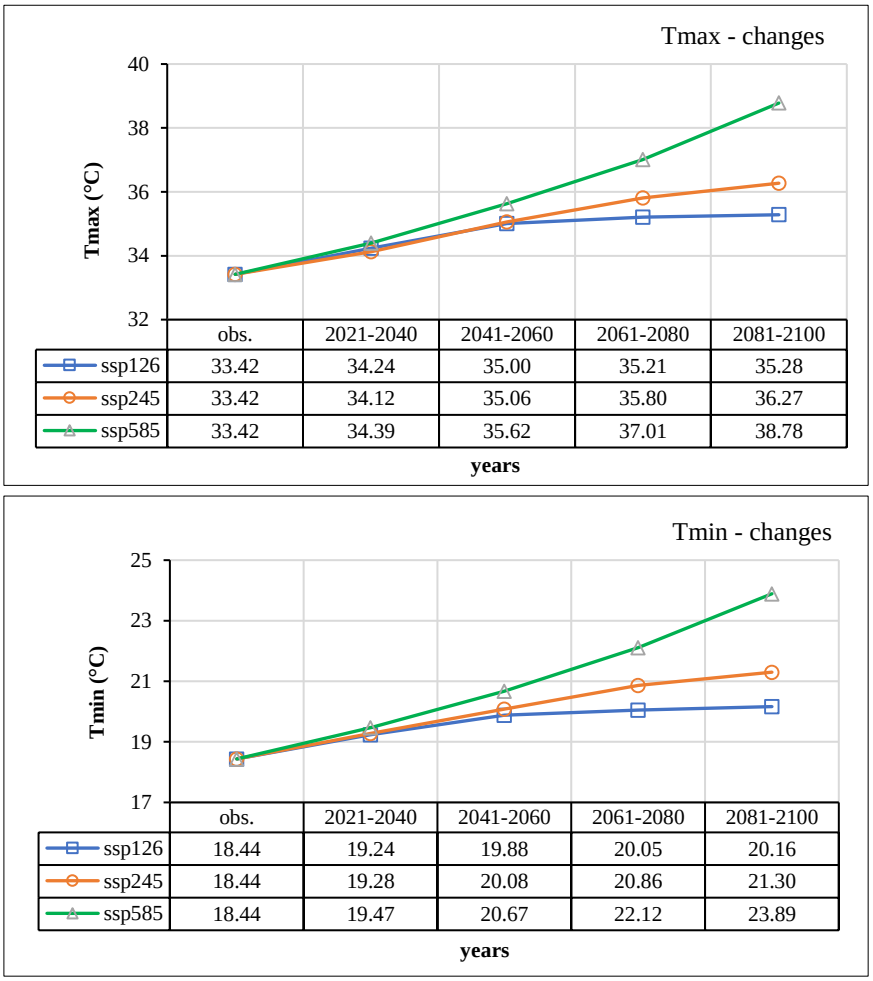

Figure 5. The trends of annual changes for MAX/MIN temperatures during future periods according to the three scenarios of the study area

Table 8. The highest mean of MAX temperature recorded through the future period

GCM	SSP126		SSP245		SSP585	
	Value	Date	Value	Date	Value	Date
ACCESS-ESM1-5	50.27		51.25	Aug-2100	53.36	Aug-2100
CNRM-CM6-1	53.03		54.14	Jul-2090	58.25	Jul-2090
HadGEM3-GC31-LL	50.41	Jul-2070	51.53	Jul-2090	54.45	Aug-2100
MPI-ESM1-2-LR	49.58		50.41	Jul-2070	52.85	Aug-2100
MRI-ESM2-0	50.08		50.89	Jul-2070	53.51	Jul-2090

Table 9. The lowest mean of MIN temperature was recorded through the future period

GCM	SSP126		SSP245		SSP585	
	Value	Date	Value	Date	Value	Date
ACCESS-ESM1-5	4.96		5.23		5.08	
CNRM-CM6-1	5.56		5.84		5.81	
HadGEM3-GC31-LL	5.24	Jan-2032	5.39	Jan-2032	6.05	Jan-2032
MPI-ESM1-2-LR	4.81		4.84		4.99	
MRI-ESM2-0	5.22		5.19		5.18	

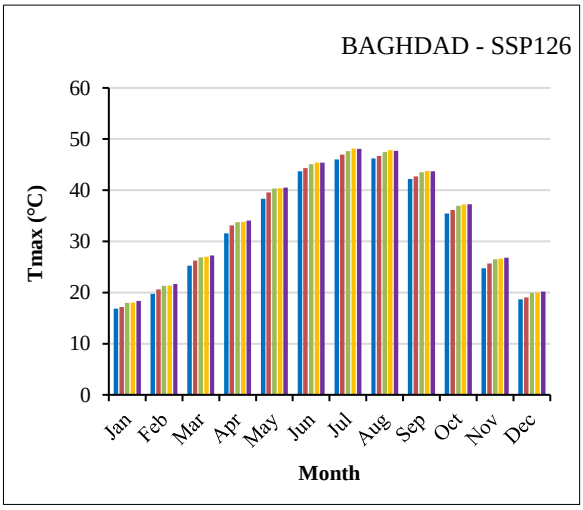

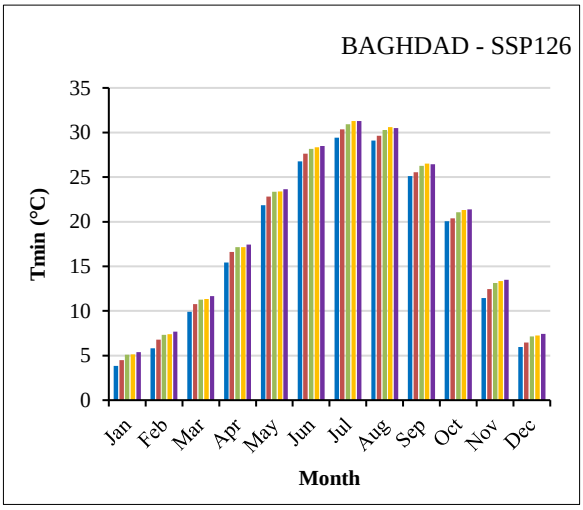

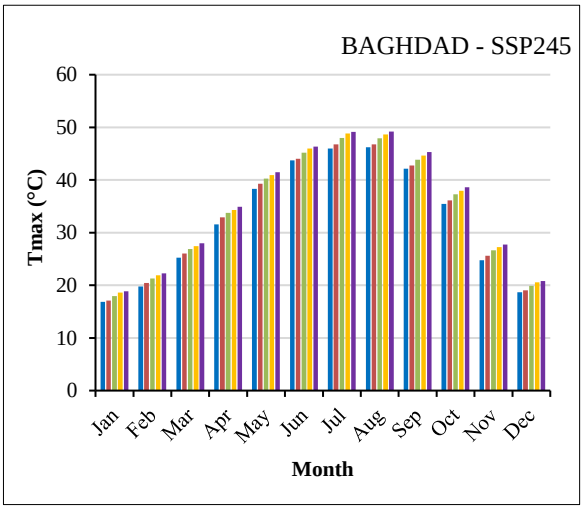

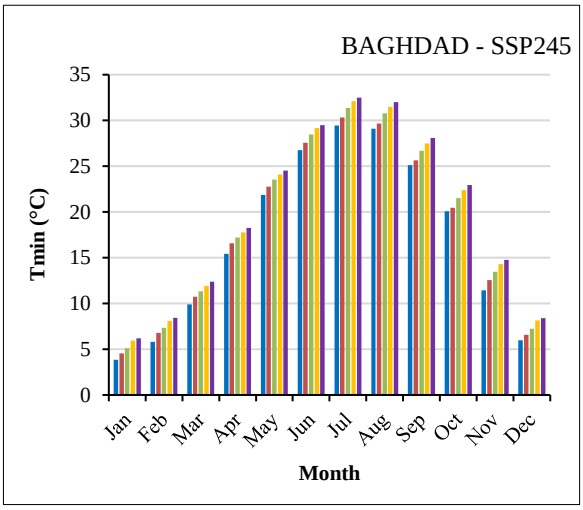

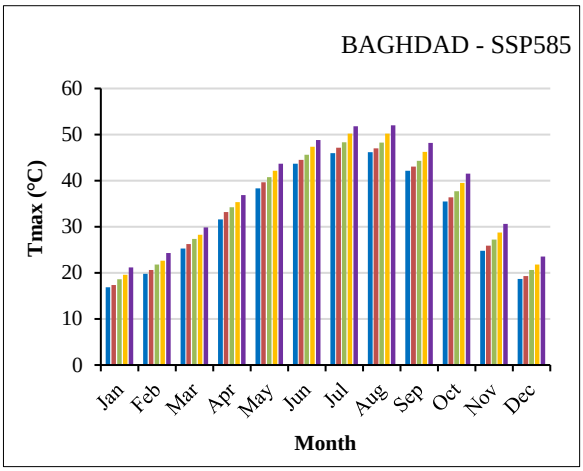
BAGHDAD - SSP585
Tmax (°C)
Month
Jan Feb Mar Apr May Jun Jul Aug Sep Oct Nov Dec

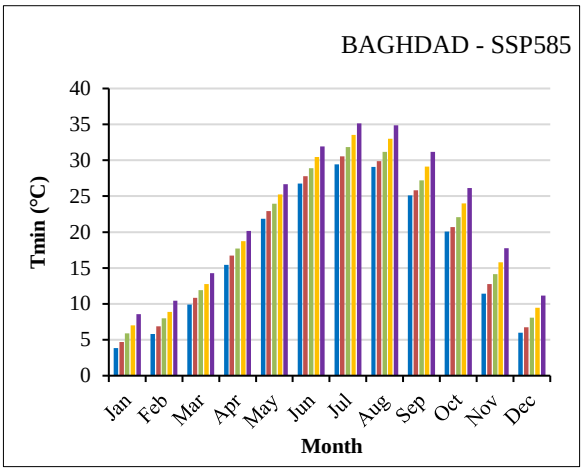
BAGHDAD - SSP585
Tmin (°C)
Month
Jan Feb Mar Apr May Jun Jul Aug Sep Oct Nov Dec

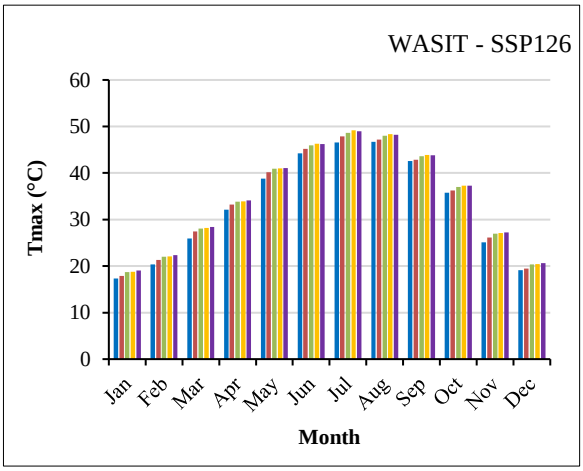
WASIT - SSP126
Tmax (°C)
Month
Jan Feb Mar Apr May Jun Jul Aug Sep Oct Nov Dec

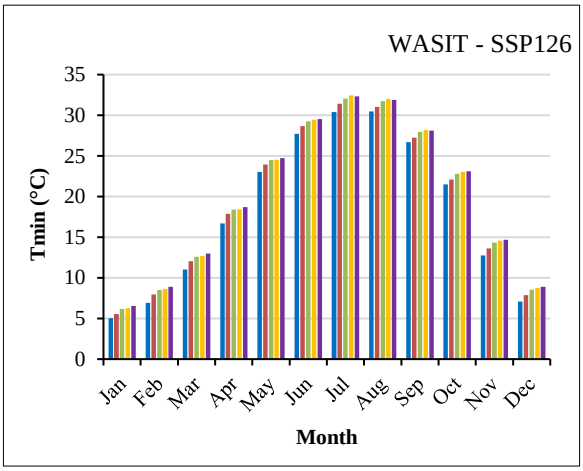
WASIT - SSP126
Tmin (°C)
Month
Jan Feb Mar Apr May Jun Jul Aug Sep Oct Nov Dec

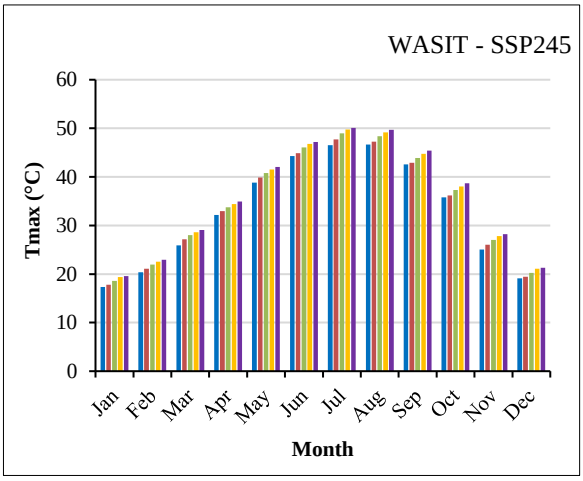
WASIT - SSP245
Tmax (°C)
Month
Jan Feb Mar Apr May Jun Jul Aug Sep Oct Nov Dec

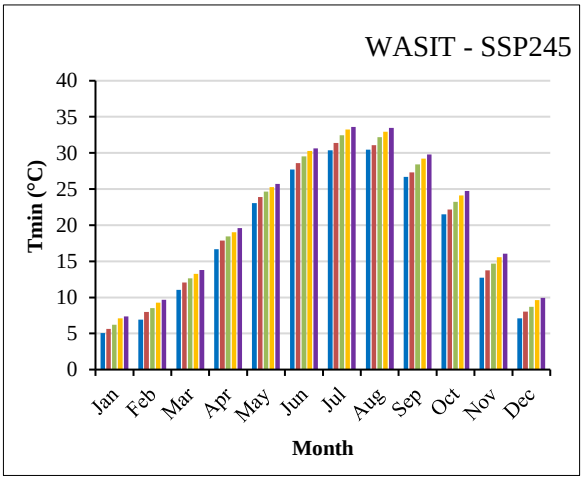
WASIT - SSP245
Tmin (°C)
Month
Jan Feb Mar Apr May Jun Jul Aug Sep Oct Nov Dec

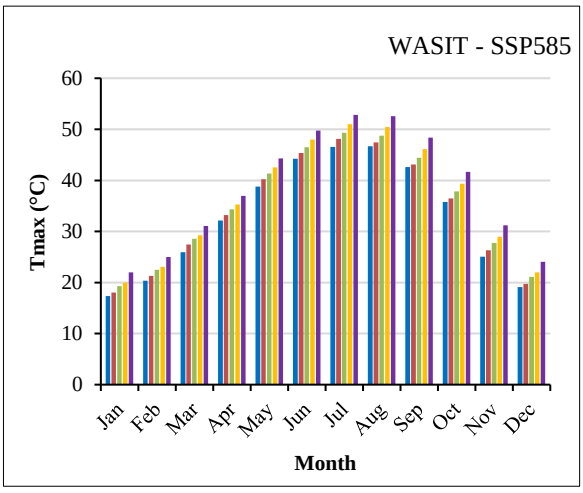
WASIT - SSP585
Tmax (°C)
Month
Jan Feb Mar Apr May Jun Jul Aug Sep Oct Nov Dec

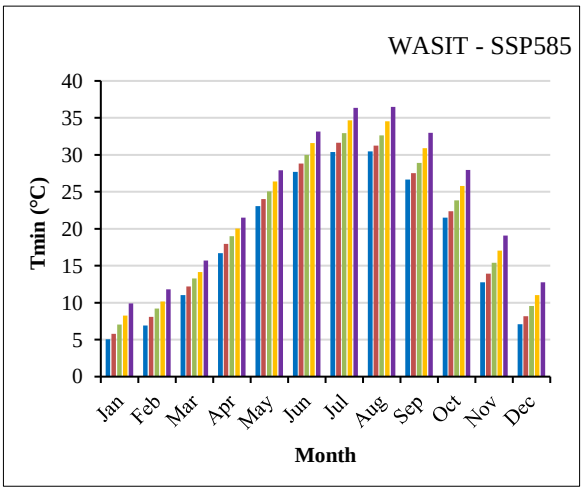
WASIT - SSP585
Tmin (°C)
Month
Jan Feb Mar Apr May Jun Jul Aug Sep Oct Nov Dec

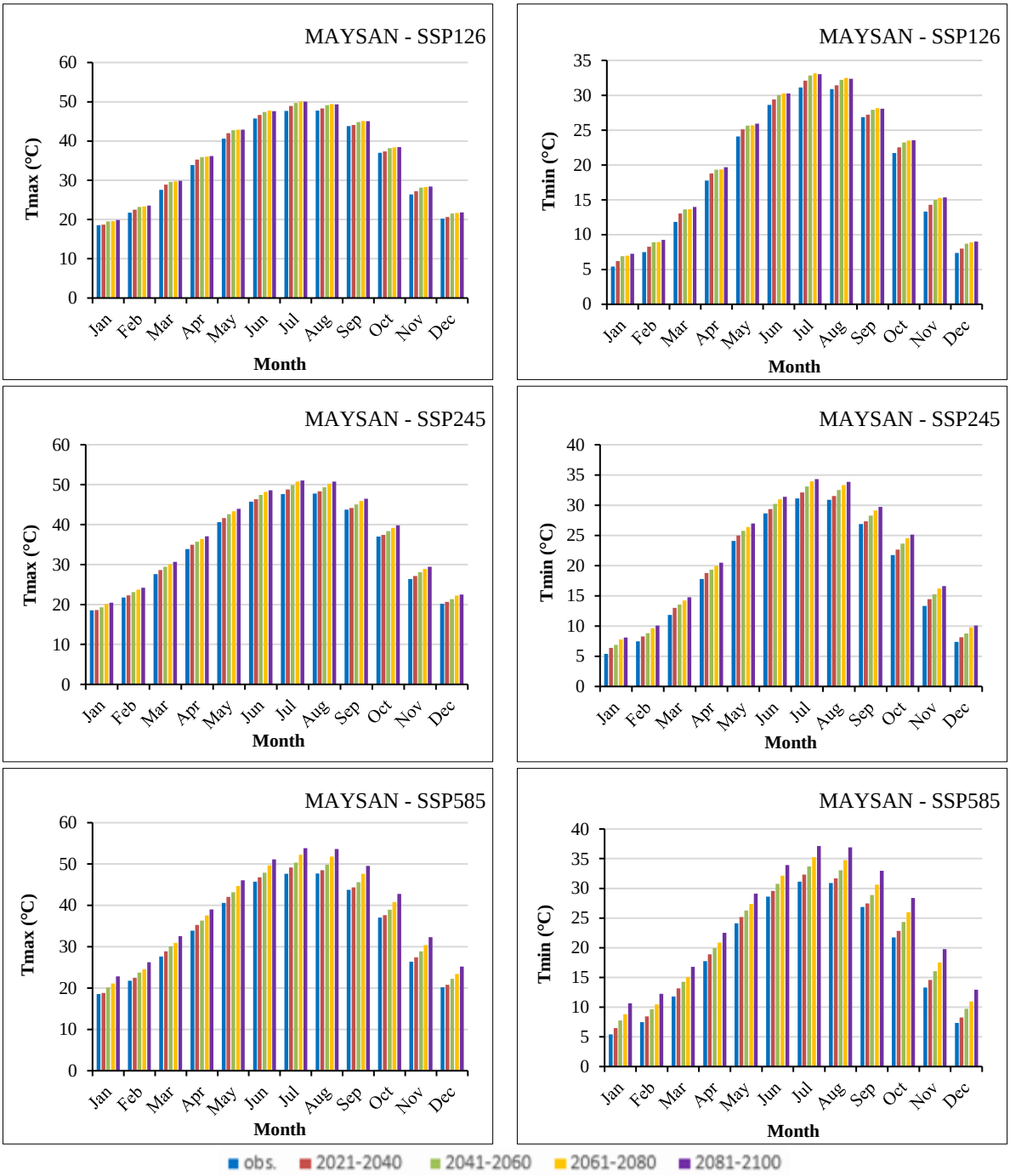

Figure 6. Comparison of observed average monthly MAX/MIN temperatures data vs. future projections under all scenarios

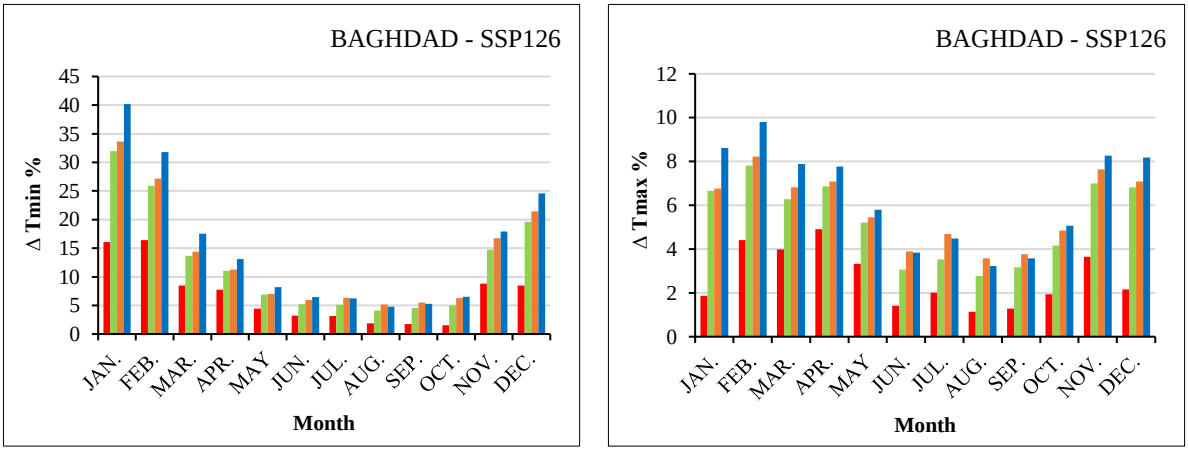

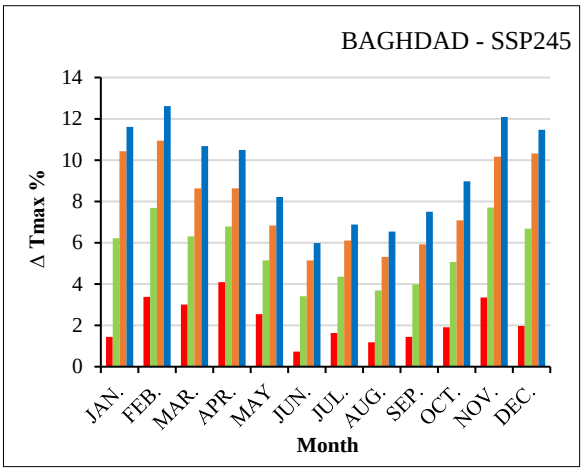
BAGHDAD - SSP245
Δ Tmax %
Month
JAN. FEB. MAR. APR. MAY JUN. JUL. AUG. SEP. OCT. NOV. DEC.

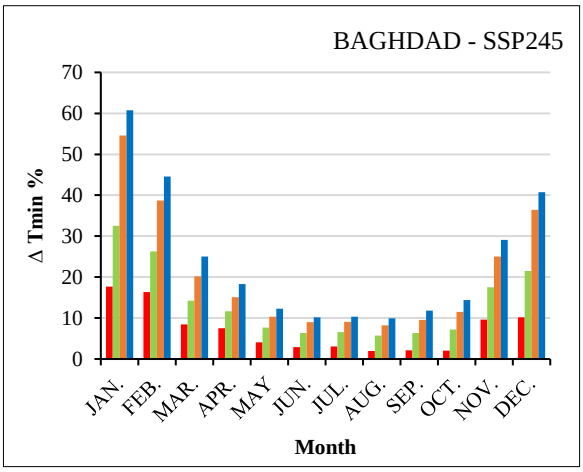
BAGHDAD - SSP245
Δ Tmin %
Month
JAN. FEB. MAR. APR. MAY JUN. JUL. AUG. SEP. OCT. NOV. DEC.

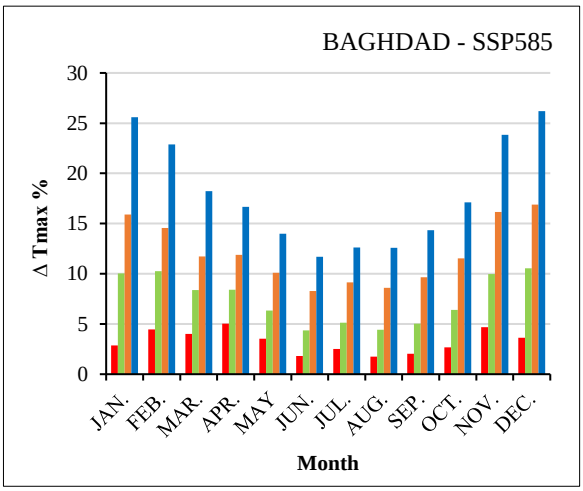
BAGHDAD - SSP585
Δ Tmax %
Month
JAN. FEB. MAR. APR. MAY JUN. JUL. AUG. SEP. OCT. NOV. DEC.

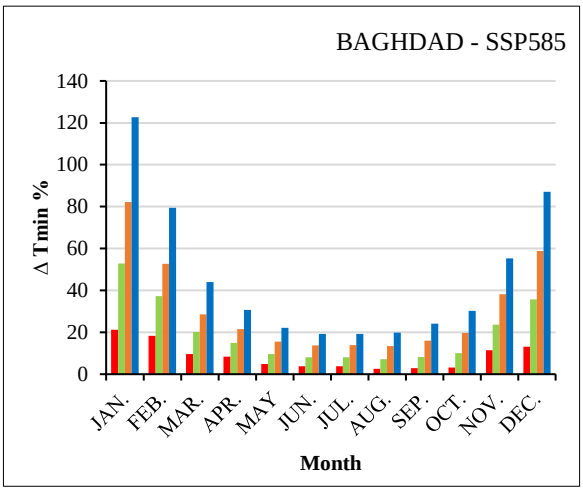
BAGHDAD - SSP585
Δ Tmin %
Month
JAN. FEB. MAR. APR. MAY JUN. JUL. AUG. SEP. OCT. NOV. DEC.

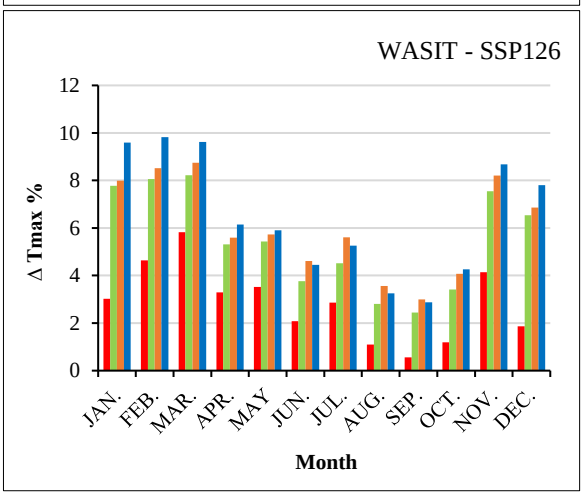
WASIT - SSP126
Δ Tmax %
Month
JAN. FEB. MAR. APR. MAY JUN. JUL. AUG. SEP. OCT. NOV. DEC.

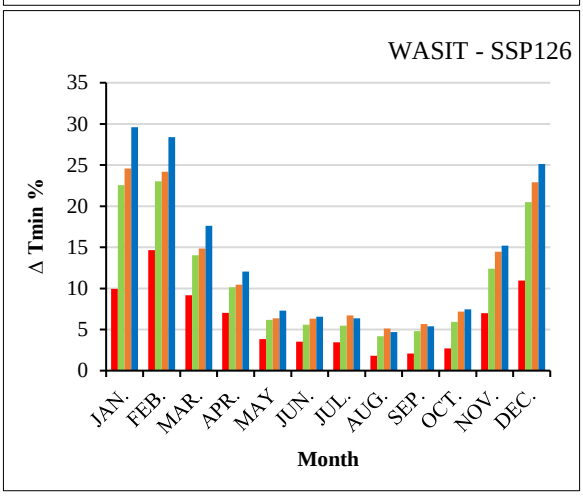
WASIT - SSP126
Δ Tmin %
Month
JAN. FEB. MAR. APR. MAY JUN. JUL. AUG. SEP. OCT. NOV. DEC.

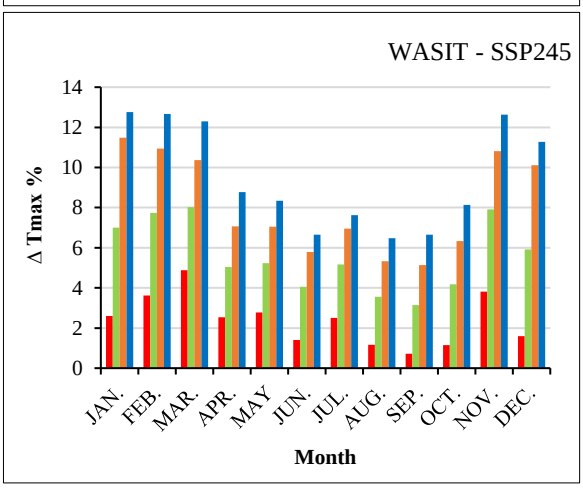
WASIT - SSP245
Δ Tmax %
Month
JAN. FEB. MAR. APR. MAY JUN. JUL. AUG. SEP. OCT. NOV. DEC.

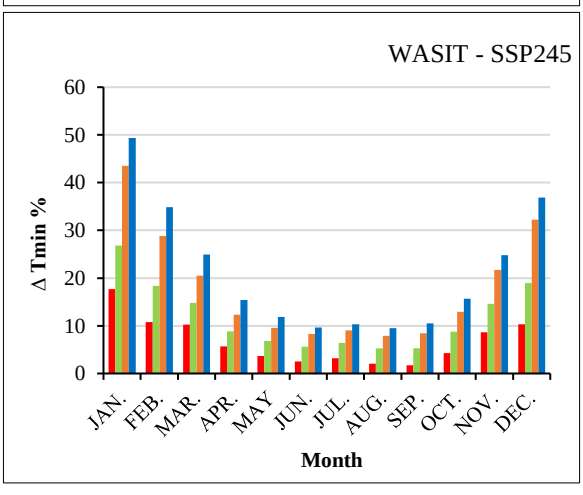
WASIT - SSP245
Δ Tmin %
Month
JAN. FEB. MAR. APR. MAY JUN. JUL. AUG. SEP. OCT. NOV. DEC.

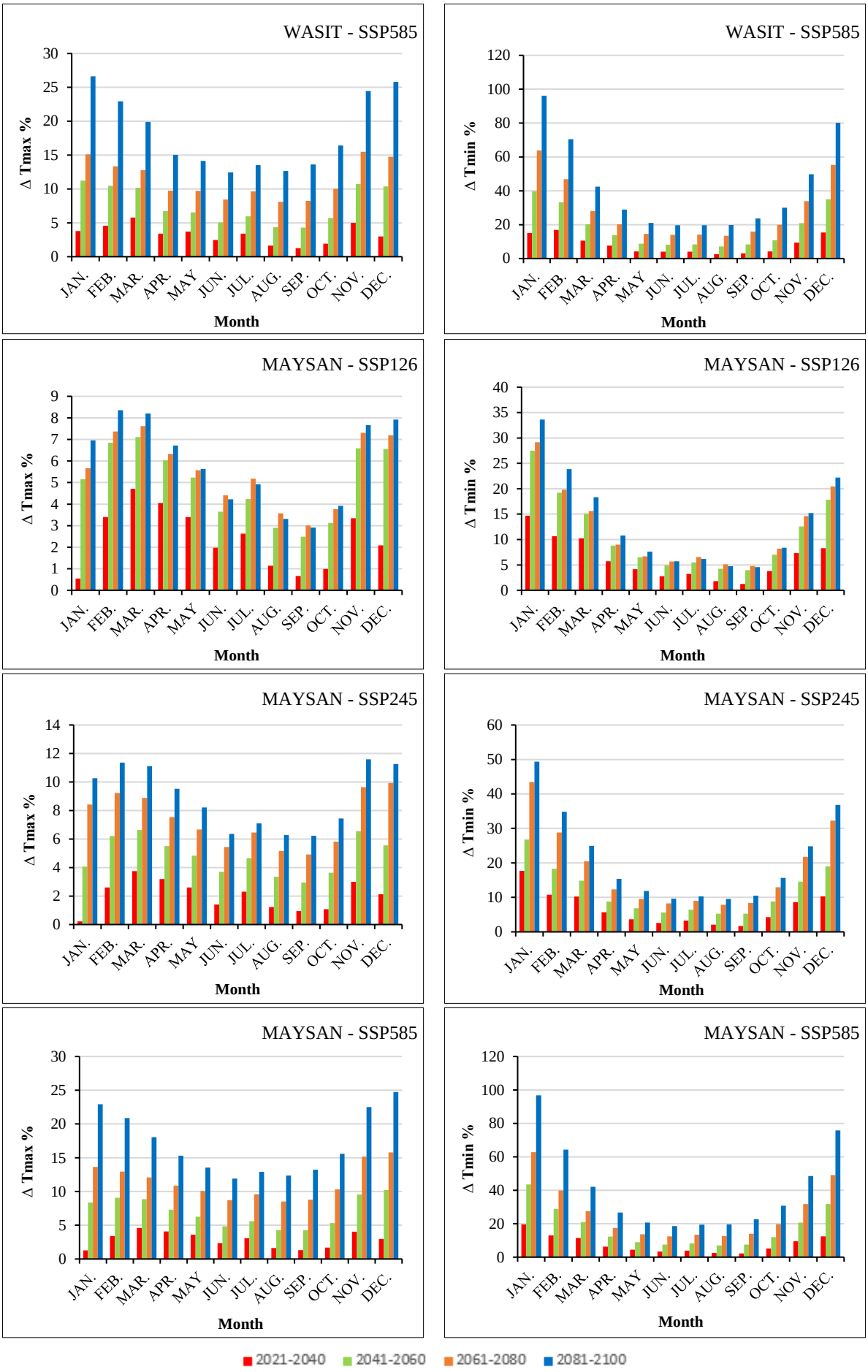

Figure 7. Relative change in average annual MAX/MIN temperatures

Figure 8 shows the future average monthly MAX/MIN temperatures from the five GCMs under the three scenarios of the selected stations. It is demonstrated that the Wasit station recorded the highest predicted estimate of monthly MAX temperatures according to the CNRM-CM6-1 model under scenario SSP585, with a difference of 7.5 °C from what was observed during the baseline. It was followed by Maysan station, then Baghdad station, with a slight difference recorded as 7.28 and 7.45 °C, respectively (Tables 8 and 9). The MAX/MIN temperatures continued to increase according to the CNRM-CM6-1 model, followed by the HadGEM3-GC31-LL model. In contrast, the MPI-ESM1-2-LR model remained the lowest among all five GCMs, which recorded 4.3, 4.41, and 4.36 °C at Baghdad, Wasit, and Maysan stations, respectively (Figure 8).

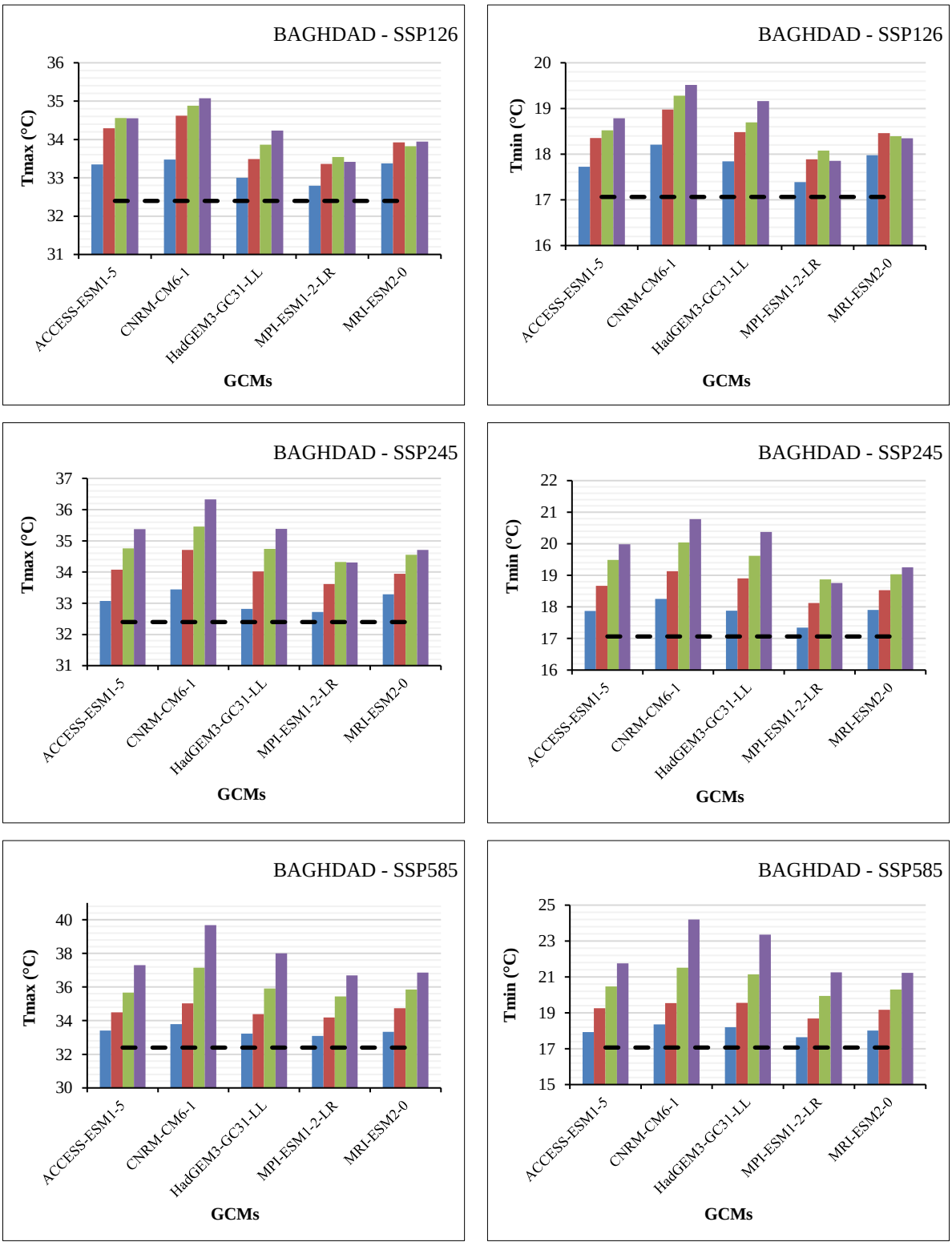

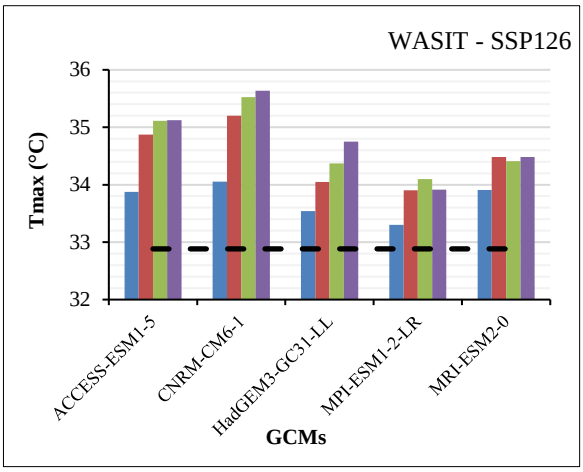
WASIT - SSP126
Tmax (°C)
36
35
34
33
32
ACCESS-ESM1-5
CNRM-CM6-1
HadGEM3-GC31-LL
MPI-ESM1-2-LR
MRI-ESM2-0
GCMs

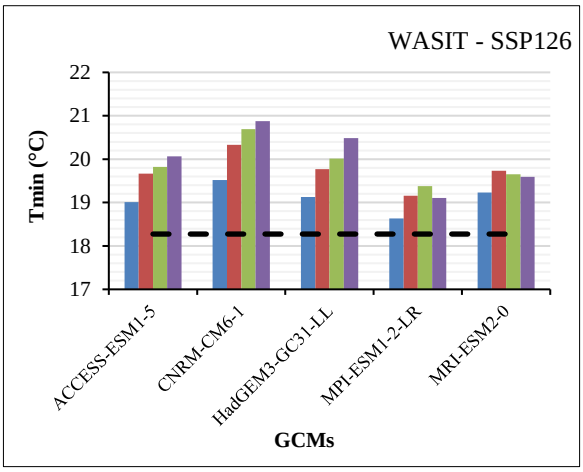
WASIT - SSP126
Tmin (°C)
22
21
20
19
18
17
ACCESS-ESM1-5
CNRM-CM6-1
HadGEM3-GC31-LL
MPI-ESM1-2-LR
MRI-ESM2-0
GCMs

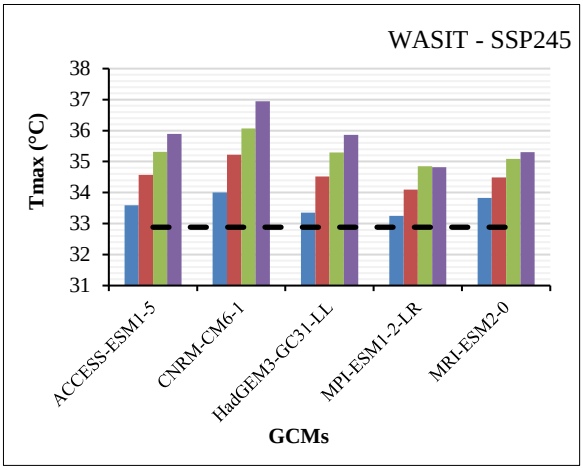
WASIT - SSP245
Tmax (°C)
38
37
36
35
34
33
32
31
ACCESS-ESM1-5
CNRM-CM6-1
HadGEM3-GC31-LL
MPI-ESM1-2-LR
MRI-ESM2-0
GCMs

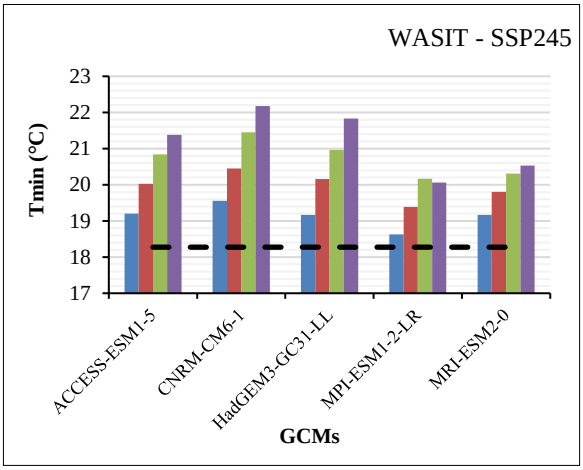
WASIT - SSP245
Tmin (°C)
23
22
21
20
19
18
17
ACCESS-ESM1-5
CNRM-CM6-1
HadGEM3-GC31-LL
MPI-ESM1-2-LR
MRI-ESM2-0
GCMs

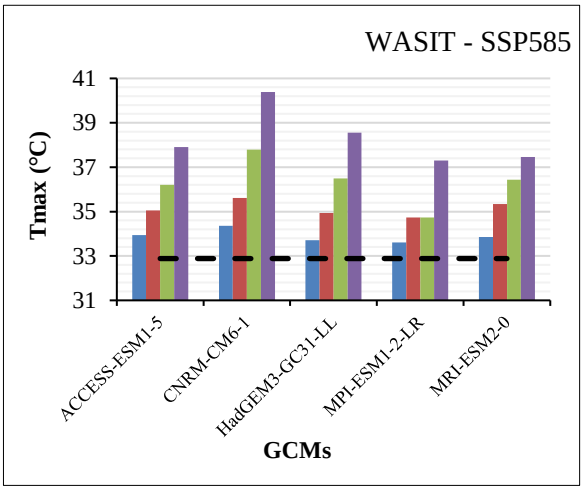
WASIT - SSP585
Tmax (°C)
41
39
37
35
33
31
ACCESS-ESM1-5
CNRM-CM6-1
HadGEM3-GC31-LL
MPI-ESM1-2-LR
MRI-ESM2-0
GCMs

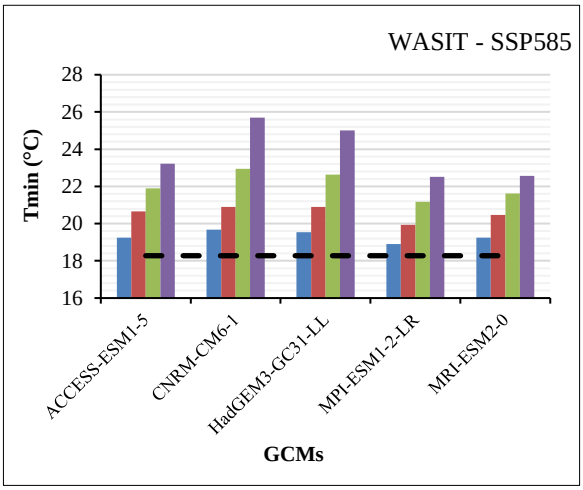
WASIT - SSP585
Tmin (°C)
28
26
24
22
20
18
16
ACCESS-ESM1-5
CNRM-CM6-1
HadGEM3-GC31-LL
MPI-ESM1-2-LR
MRI-ESM2-0
GCMs

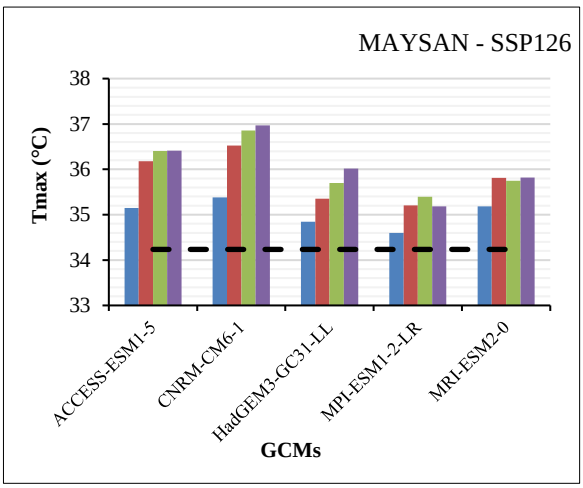
MAYSAN - SSP126
Tmax (°C)
38
37
36
35
34
33
ACCESS-ESM1-5
CNRM-CM6-1
HadGEM3-GC31-LL
MPI-ESM1-2-LR
MRI-ESM2-0
GCMs

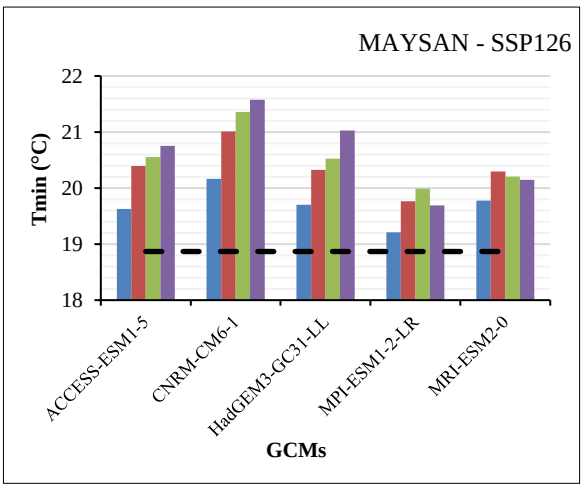
MAYSAN - SSP126
Tmin (°C)
22
21
20
19
18
ACCESS-ESM1-5
CNRM-CM6-1
HadGEM3-GC31-LL
MPI-ESM1-2-LR
MRI-ESM2-0
GCMs

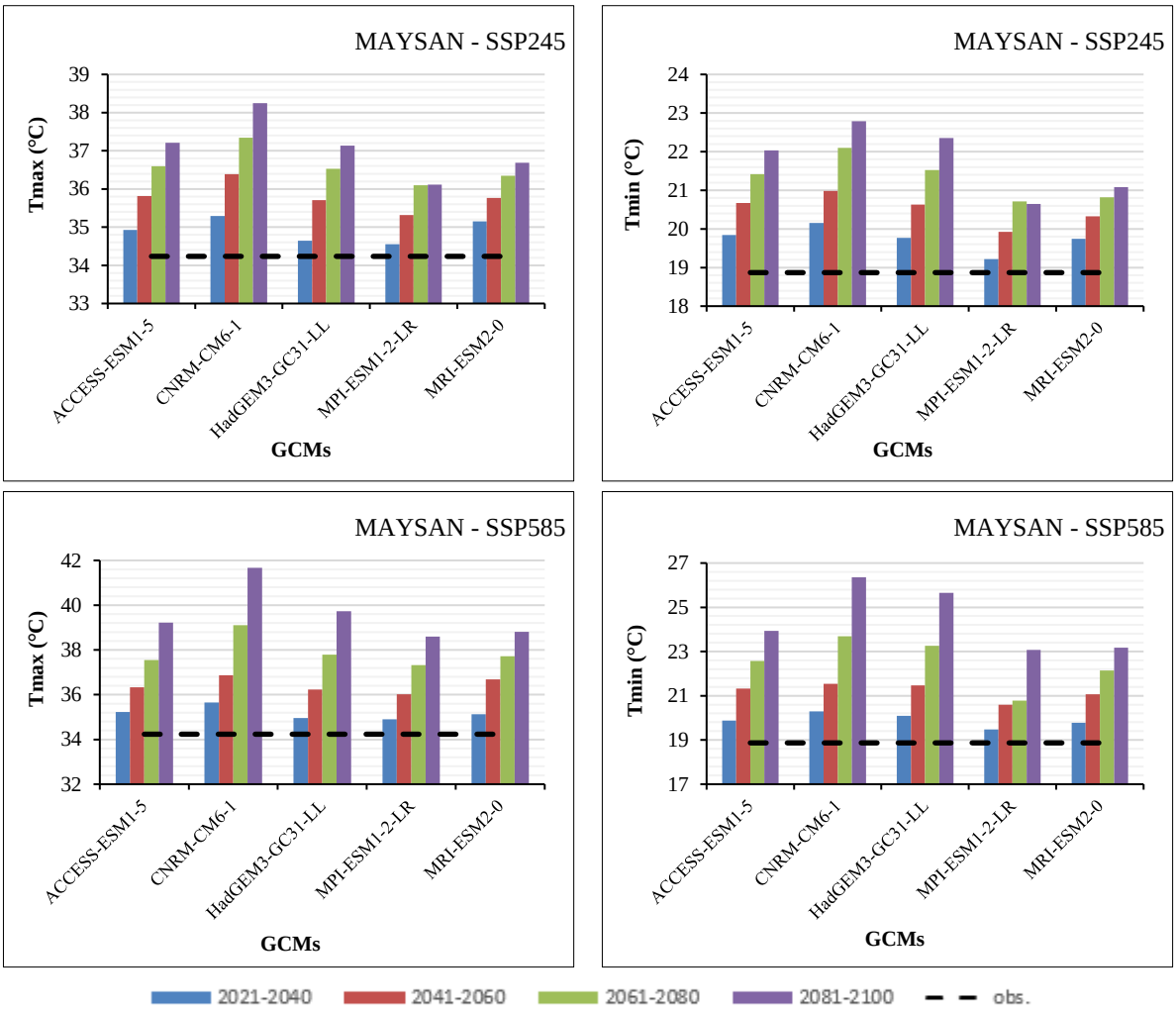

Figure 8. Comparison of future average monthly MAX / MIN temperatures by using five GCMs under the three scenarios

3.3. Precipitation Projection in the Future

The five GCMs proved varying results in precipitation under the three scenarios adopted in this study. The fluctuations in precipitation occur due to their continuous variation between time periods and different locations, which records missing data during the months of the year due to its non-occurrence, especially in the summer season during June, July, and August. This implies that using an individual model will increase the uncertainty of the forecasted results, so it requires adopting different models in predicting future precipitation. In this study, the results of the precipitation average varied in some future periods. However, the potential trends in precipitation across the entire study area will increase at the end of the current century but slightly compared to the base period, as shown in Figure 9. The SSP585 scenario represents the highest record of future precipitation projections compared to other scenarios; the highest precipitation in future forecasts results during the period 2081-2100, which will occur in December, January, and February (the winter season) and will fluctuate in the spring and autumn seasons, while it will almost disappear in June, July, and August (the summer season). This is normal since Iraq is characterized by its dry climate, as presented by Al-Maliki et al. [36]. Especially in the southern governorates. Figure 10 shows the relative change in precipitation between future and observed periods from the five GCMs. In all scenarios, there is a fluctuating variation in the occurrence of precipitation in Baghdad, while in Wasit Maysan, it will decrease in all months except October, in which the incidence of precipitation will be higher than recorded in the historical period. It is also noticed that there is a fluctuation in precipitation even in the same model and scenario, as shown in Figure 11. For instance, according to the HadGEM3-GC31-LL model, the highest values of the annual average precipitation of 14.5, 18.5, 17.79, and 19.33 mm were recorded for the periods 2021-2040, 2041-2060, 2061-2080, and 2081-2100, respectively, in the SSP126 scenario at the Baghdad station. This applies to the rest of the sites, GCMs, and scenarios. However, it was found that the HadGEM3-GC31-LL model, in all scenarios, had the highest record of future forecasts of precipitation in the coming periods until the end of the century. In contrast, it was found in the MPI-ESM1-2-LR model, which is quite the opposite. It had the lowest record of precipitation data. The location in Wasit had the highest and lowest annual precipitation rates, which were 20.36 and 8.46 mm in the same scenario, SSP585, then followed by Maysan and Baghdad.

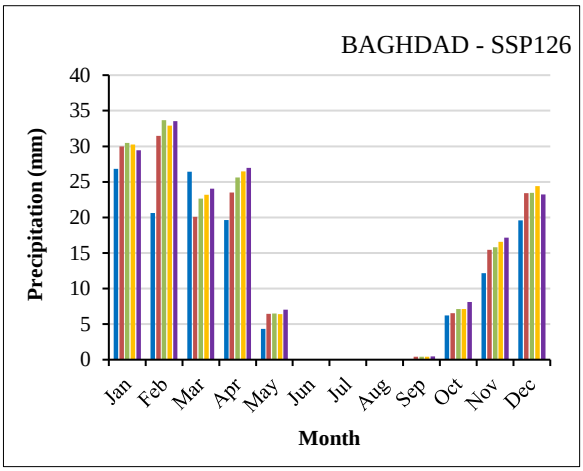
BAGHDAD - SSP126
Precipitation (mm)
Month
Jan Feb Mar Apr May Jun Jul Aug Sep Oct Nov Dec

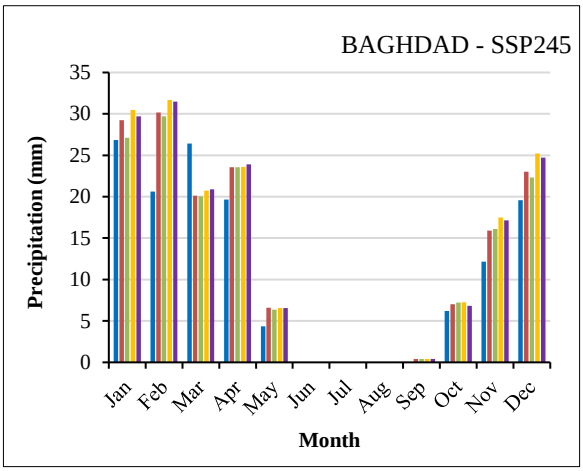
BAGHDAD - SSP245
Precipitation (mm)
Month
Jan Feb Mar Apr May Jun Jul Aug Sep Oct Nov Dec

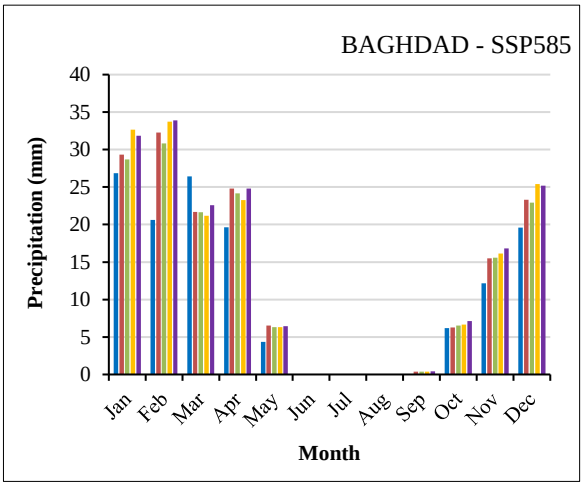
BAGHDAD - SSP585
Precipitation (mm)
Month
Jan Feb Mar Apr May Jun Jul Aug Sep Oct Nov Dec

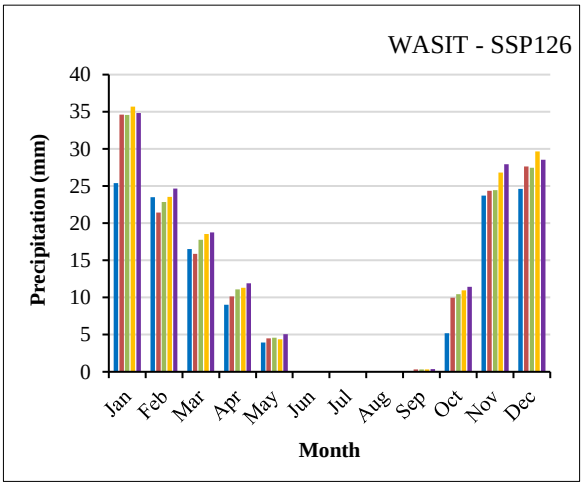
WASIT - SSP126
Precipitation (mm)
Month
Jan Feb Mar Apr May Jun Jul Aug Sep Oct Nov Dec

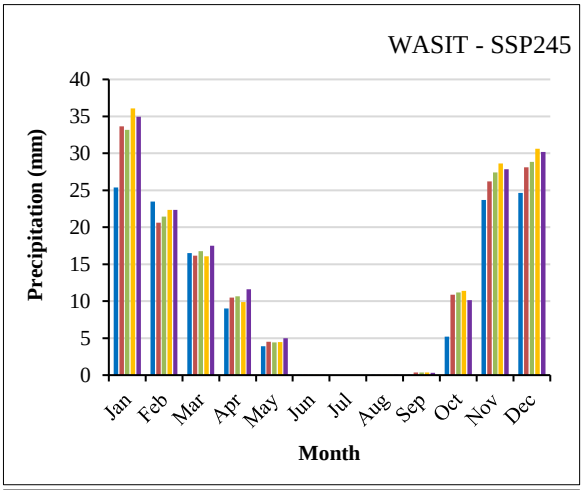
WASIT - SSP245
Precipitation (mm)
Month
Jan Feb Mar Apr May Jun Jul Aug Sep Oct Nov Dec

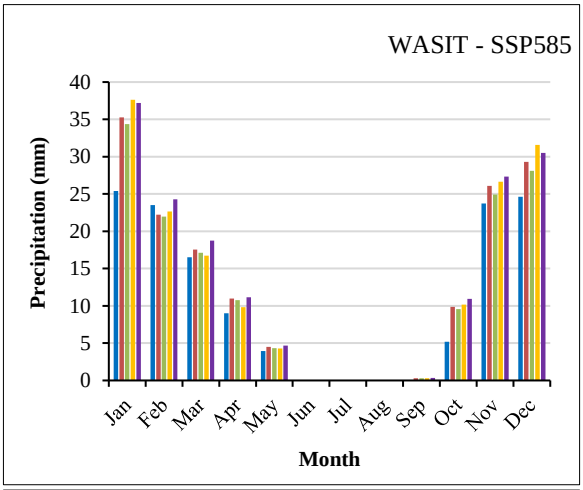
WASIT - SSP585
Precipitation (mm)
Month
Jan Feb Mar Apr May Jun Jul Aug Sep Oct Nov Dec

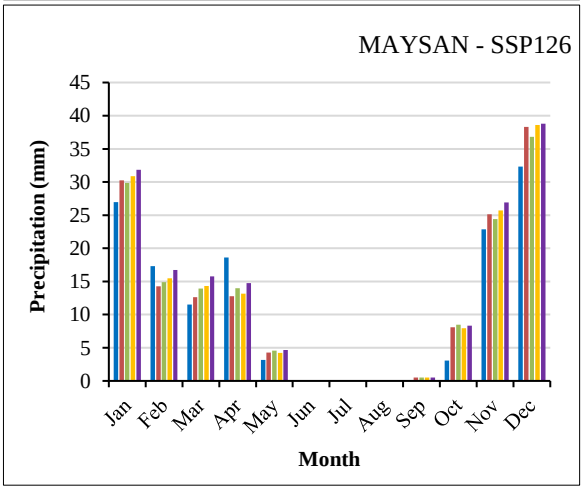
MAYSAN - SSP126
Precipitation (mm)
Month
Jan Feb Mar Apr May Jun Jul Aug Sep Oct Nov Dec

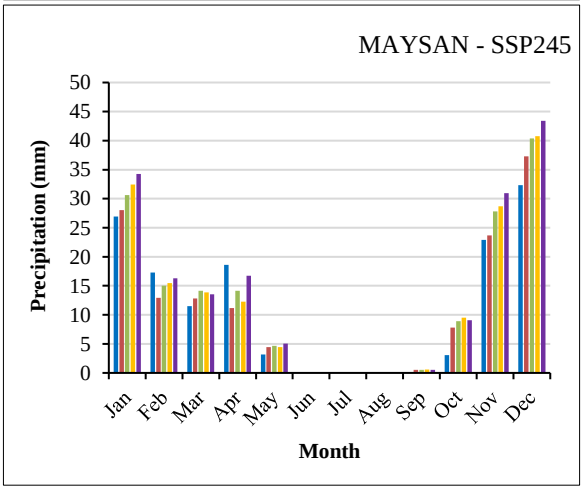
MAYSAN - SSP245
Precipitation (mm)
Month
Jan Feb Mar Apr May Jun Jul Aug Sep Oct Nov Dec

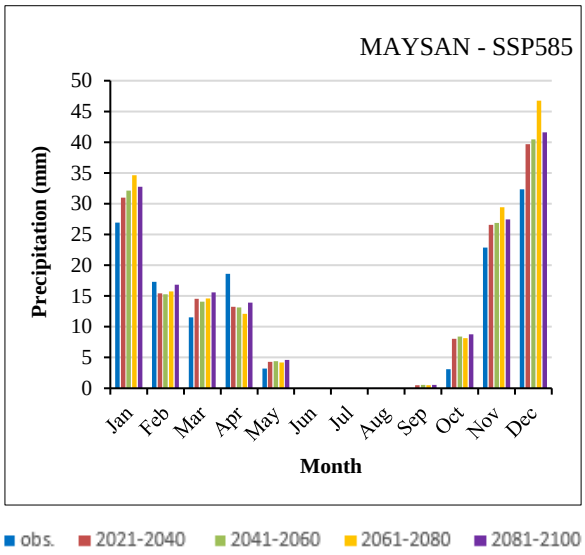

Figure 9. Comparison of observed average monthly precipitation versus future projections under all scenarios

In general, future trends in precipitation fluctuate between increases and decreases, even if the change is slight. Accordingly, the study area will experience different patterns of precipitation during the future period. Moreover, the presented results are consistent with the findings of Muheisen et al. [29, 35], Al-Hasani et al. [30], and Saeed et al. [31].

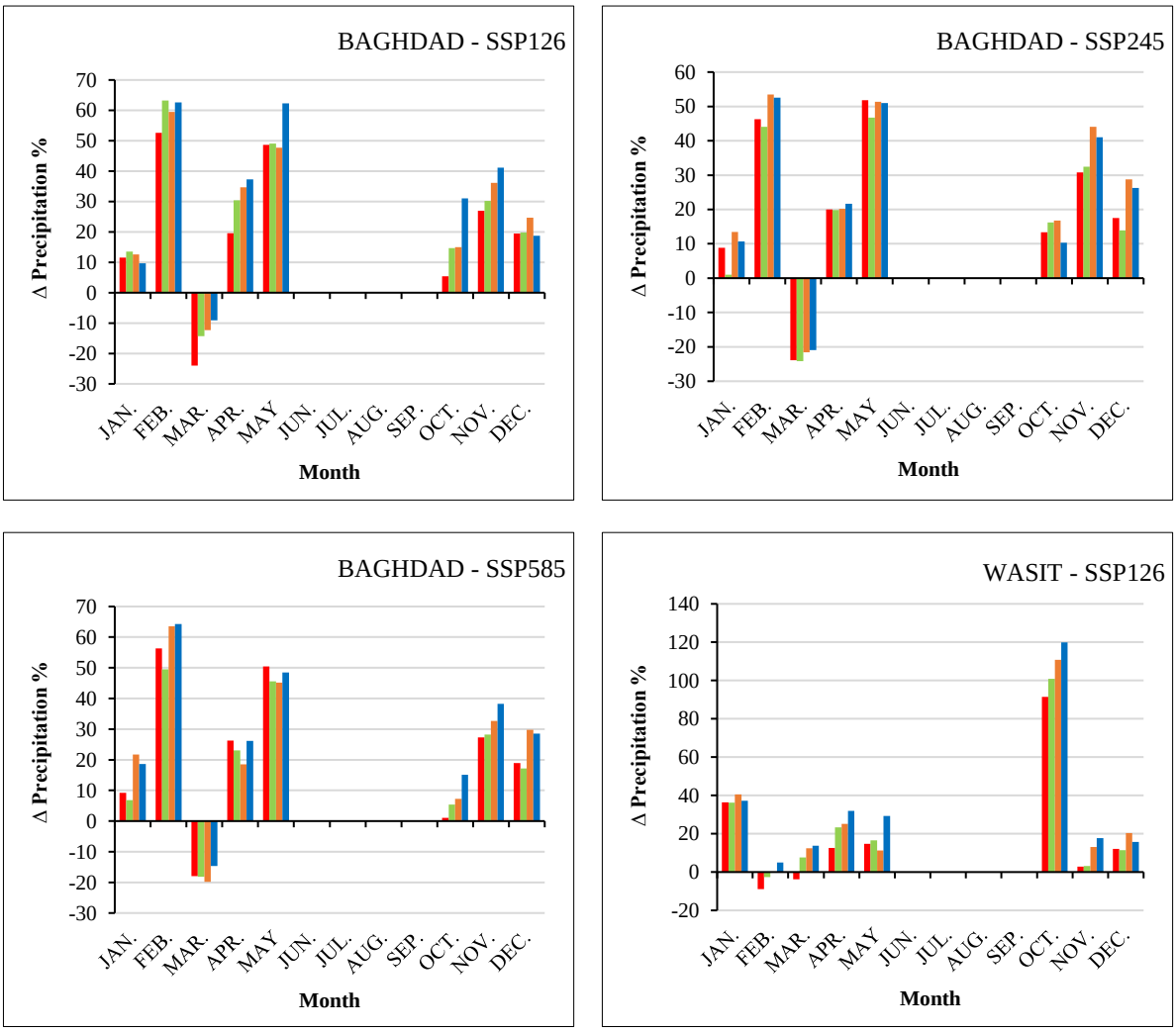

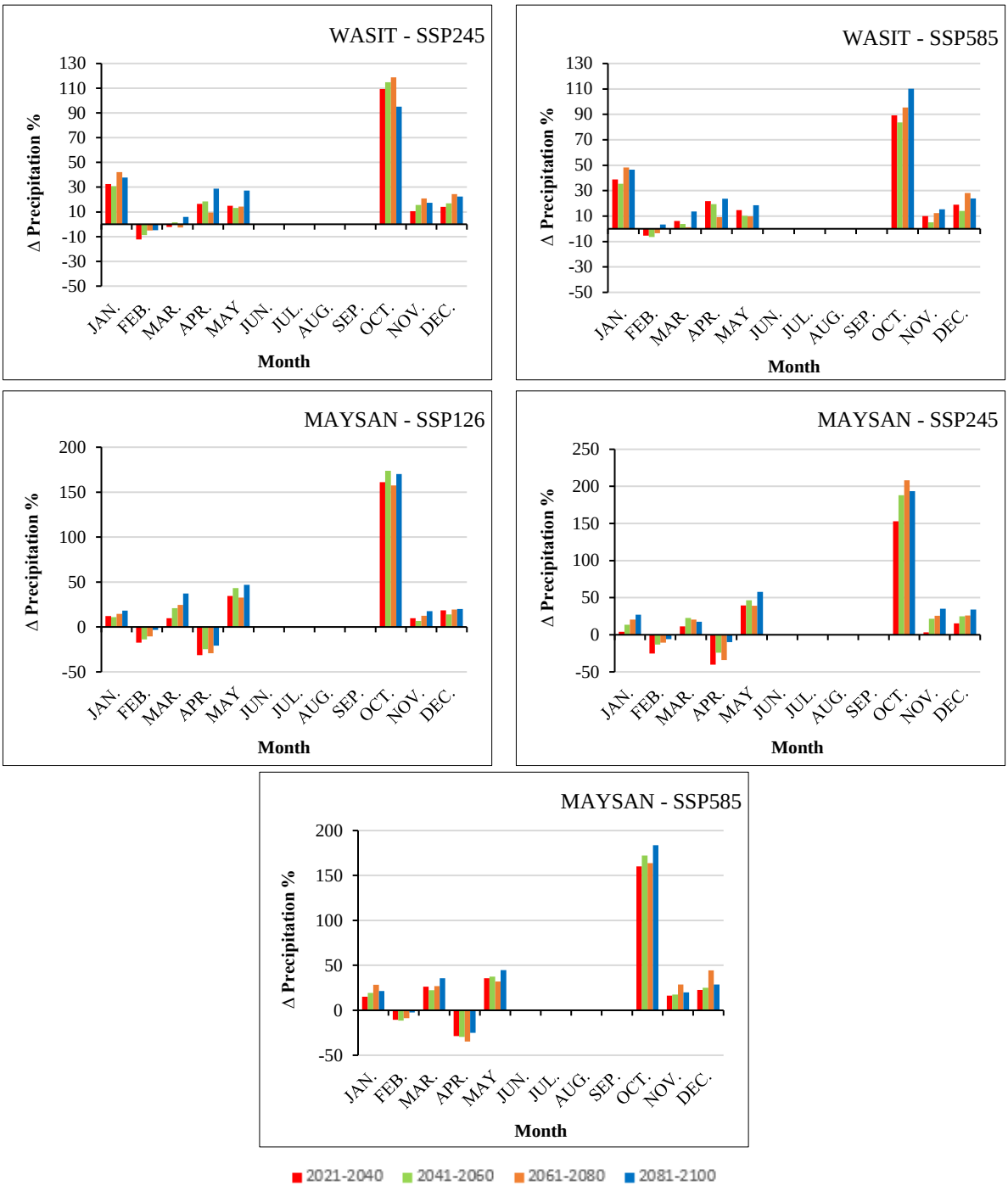

Figure 10. Relative change in average annual precipitation under all scenarios

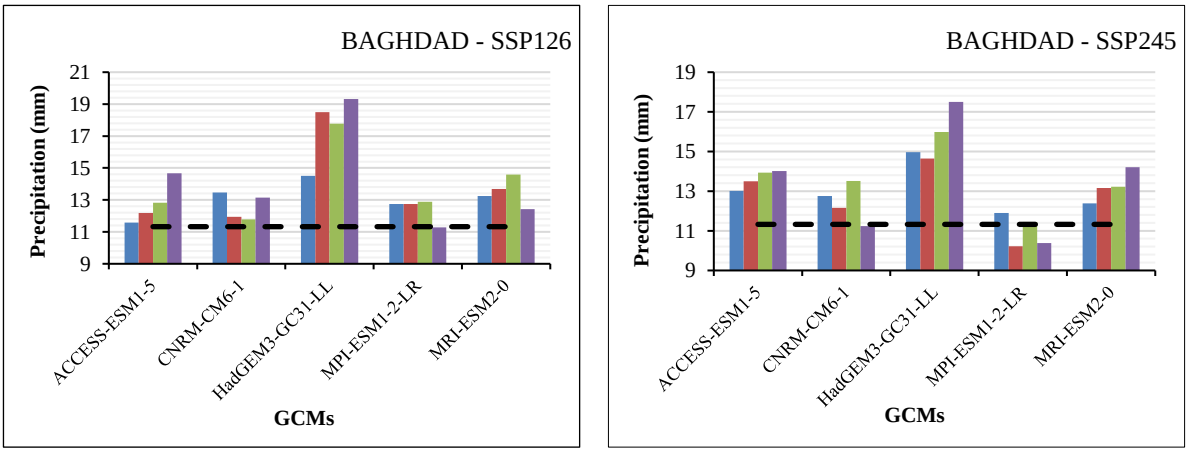

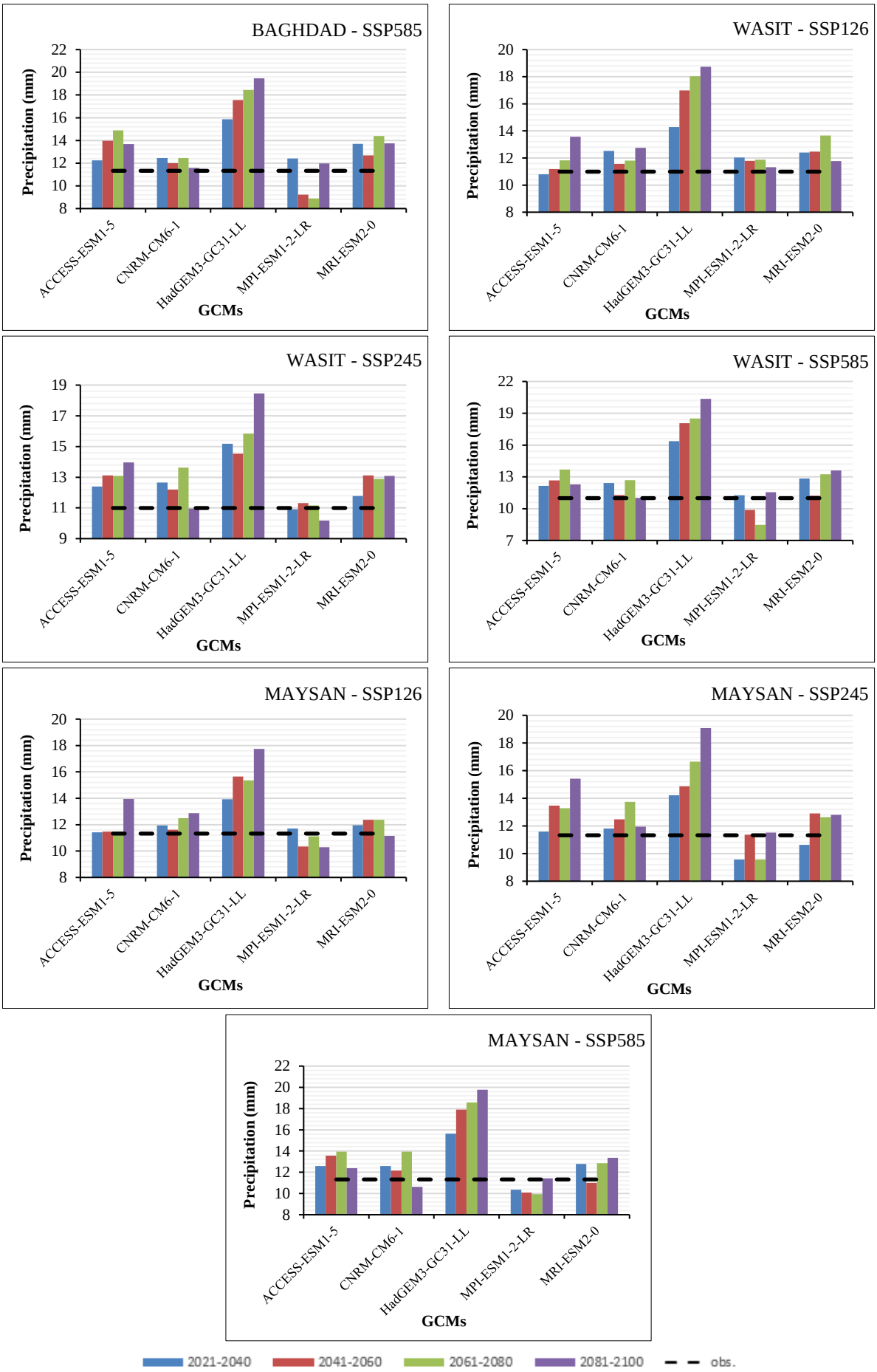

Figure 11. Comparison of observed average monthly precipitation data versus future data according to the five GCMs under the three scenarios

4. Conclusions

The climate change occurring in Iraq and its surrounding areas is a source of concern because it is located within arid and semi-arid lands that have been impacted by global climate change. This, in turn, led to an accelerated change in climate variables, especially precipitation and MAX/MIN temperatures. This study aimed to clarify and understand the behavior and trends of climate variables such as precipitation and temperatures, whether increasing, decreasing, or both. The study area, which consists of three governorates, Baghdad, Wasit, and Maysan, is located along the Tigris River basin in Iraq. The LARS-WG was evaluated to elucidate future trends for the parameters using five different GCMs, namely ACCESS-ESM1-5, CNRM-CM6-1, HadGEM3-GC31-LL, MPI-ESM1-2-LR, and MRI-ESM2-0, under the three scenarios, i.e., SSP126, SSP245, and SSP585.

It was concluded that the LARS-WG model was superior for projecting the frequency of observed precipitation and temperatures during the baseline period of 2003-2022, indicating the ability of the model to be used in the future for various scientific and practical applications. It was shown that temperature trends will be increasing and continuing until the end of the current century according to all five GCMs under the three scenarios (SSP126, SSP245, and SSP585). However, the model CNRM-CM6-1 was the highest one to project the future increase/decrease of temperatures/ precipitation among all five GCMs under the three scenarios. Mean temperatures were expected to rise above those observed at the end of the future period (2081-2100) for scenario SSP585 by 7.28, 7.5, and 7.45 °C at the Baghdad, Wasit, and Maysan stations, respectively, according to the CNRM-CM6-1 model. The MPI-ESM1-2-LR model was the lowest in projecting mean temperatures by 4.3, 4.41, and 4.36 °C at the Baghdad, Wasit, and Maysan stations, respectively. Therefore, it is recommended that several GCMs be used in future forecasts to reduce uncertainty. For precipitation, the results showed a clear fluctuation during the months of the year according to all GCMs under the three scenarios. However, the LARS-WG8.0 model gave a clear interpretation by recording the highest amount of precipitation during the winter season, which was in December, January, and February of each year. The results showed fluctuations in the spring and autumn seasons. Still, it was poor in the summer, particularly in June, July, and August, which are among the hottest months in Iraq and its neighboring regions. The highest mean precipitation was recorded according to the HadGEM3-GC31-LL model. The MPI-ESM1-2-LR model was the opposite.

Therefore, the changes in climate variables will negatively impact water and agricultural resources. This impact will extend to a broader ambit on the economic side and socially concerning increasing population and urban expansion, accompanied by an increase in drought, desertification, and water scarcity due to the continuous rise in temperatures and fluctuations in precipitation, which will influence economic and social factors. Accordingly, this study helps those interested in this field in reading the future visualization of the study area and adapting suitable measures to mitigate the negative consequences of climate changes.

5. List of Abbreviations

(K-S) test	Kolmogorov-Smirnov tests	R	Pearson Correlation Coefficient
AR6	Sixth assessment report	R^2	Determination Coefficient
Av	Average	RCP	Representative concentration pathway
°C	Celsius degree	RMSE	Root Mean Square Error
CHIRPS	Climate hazards group infrared precipitation with station data	SD	Standard Deviation
CMIP	Climate Model Intercomparison Project	Sim	Simulated
DJF	December, January, and February	SON	September, October, and November
F-test	F-Test Statistic	SSP	Shared socio-economic pathway
GCMs	Global Climate Models	Temp	temperature
IPCC	Intergovernmental Panel on Climate Change	T_{max}	Maximum Temperature
JJA	June, July, and August	T_{min}	Minimum Temperature
LARS-WG	Long Ashton Research Station Weather Generator	T-test	Hypothesis Test Statistic
Lat	Latitude	UK	United Kingdom
Long	Longitude	X_i	Any variable rank in the time series
MAM	March, April, and May	X_{obs}	Observed Variable
MAX	Maximum	X_0	Minimum of X_{obs}
MIN	Minimum	X_n	Maximum of X_{obs}
N	Number of tests	n	The last rank of the variable values
NASA	National Aeronautics and Space Administration	P_i	The probability distribution for X_i
NSE	Nash-Sutcliff Efficiency	P_0	The probability distribution for X_0
Obs	Observed	P_n	The probability distribution for X_n
P	Probability		

6. Declarations

6.1. Author Contributions

Conceptualization, M.A., M.M., and K.S.; methodology, M.M. and K.S.; software, M.A.; data processing, M.A. and M.M.; validation, M.A.; investigation, M.A. and K.S.; resources, K.S. and M.A.; writing—original draft preparation, M.A., M.M., and K.S.; writing—editing, and reviewing, M.A., M.M., and K.S.; visualizing, M.A., M.M., and K.S.; supervision, M.M. and K.S.; Project management, M.A., M.M., and K.S. All authors have read and agreed to the published version of the manuscript.

6.2. Data Availability Statement

The data presented in this study are available in the article.

6.3. Funding and Acknowledgements

The authors would like to thank the Iraqi Ministry of Water Resources - General Commission for Irrigation and Reclamation Projects, for funding this research. This study is part of specialized scientific studies in the field of water resources in Iraq under climate change and its future impacts.

6.4. Conflicts of Interest

The authors declare no conflict of interest.

7. References

[1] Al-Mukhtar, M., Dunger, V., & Merkel, B. (2014). Evaluation of the climate generator model CLIGEN for rainfall data simulation in Bautzen catchment area, Germany. Hydrology Research, 45(4–5), 615–630. doi:10.2166/nh.2013.073.

[2] Jabal, Z. K., Khayyun, T. S., & Alwan, I. A. (2022). Impact of Climate Change on Crops Productivity Using MODIS-NDVI Time Series. Civil Engineering Journal (Iran), 8(6), 1136–1156. doi:10.28991/CEJ-2022-08-06-04.

[3] Sabah, N., Al-Mukhtar, M., & Shemal, K. (2023). Implementing Management Practices for Enhancing Water-Food Nexus Under Climate Change. Civil Engineering Journal (Iran), 9(12), 3108–3122. doi:10.28991/CEJ-2023-09-12-010.

[4] Sissakian, V. K., Jassim, H. M., Adamo, N., & Ansari, N. Al. (2022). Consequences of the Climate Change in Iraq. Global Journal of Human-Social Science, 22(2), 13–25. doi:10.34257/gjhssbvol22is2pg13.

[5] Rogelj, J., Popp, A., Calvin, K. V., Luderer, G., Emmerling, J., Gernaat, D., Fujimori, S., Strefler, J., Hasegawa, T., Marangoni, G., Krey, V., Kriegler, E., Riahi, K., Van Vuuren, D. P., Doelman, J., Drouet, L., Edmonds, J., Fricko, O., Harmsen, M., … Tavoni, M. (2018). Scenarios towards limiting global mean temperature increase below 1.5 °c. Nature Climate Change, 8(4), 325–332. doi:10.1038/s41558-018-0091-3.

[6] Riahi, K., van Vuuren, D. P., Kriegler, E., Edmonds, J., O'Neill, B. C., Fujimori, S., Bauer, N., Calvin, K., Dellink, R., Fricko, O., Lutz, W., Popp, A., Cuaresma, J. C., KC, S., Leimbach, M., Jiang, L., Kram, T., Rao, S., Emmerling, J., … Tavoni, M. (2017). The Shared Socioeconomic Pathways and their energy, land use, and greenhouse gas emissions implications: An overview. Global Environmental Change, 42, 153–168. doi:10.1016/j.gloenvcha.2016.05.009.

[7] Touzé-Peiffer, L., Barberousse, A., & Le Treut, H. (2020). The Coupled Model Intercomparison Project: History, uses, and structural effects on climate research. Wiley Interdisciplinary Reviews: Climate Change, 11(4), 648. doi:10.1002/wcc.648.

[8] Hassan, W. H., & Nile, B. K. (2021). Climate change and predicting future temperature in Iraq using CanESM2 and HadCM3 modeling. Modeling Earth Systems and Environment, 7(2), 737–748. doi:10.1007/s40808-020-01034-y.

[9] Namdar, R., Karami, E., & Keshavarz, M. (2021). Climate change and vulnerability: The case of MENA countries. ISPRS International Journal of Geo-Information, 10(11), 794. doi:10.3390/ijgi10110794.

[10] Javadinejad, S., Dara, R., & Jafary, F. (2020). Climate change scenarios and effects on snow-melt runoff. Civil Engineering Journal, 6(9), 1715–1725. doi:10.28991/cej-2020-03091577.

[11] Adamo, N., Al-Ansari, N., Sissakian, V., Fahmi, K. J., & Abed, S. A. (2022). Climate Change: Droughts and Increasing Desertification in the Middle East, with Special Reference to Iraq. Engineering, 14(07), 235–273. doi:10.4236/eng.2022.147021.

[12] Tarawneh, Q., & Chowdhury, S. (2018). Trends of Climate Change in Saudi Arabia: Implications on Water Resources. Climate, 6(1), 8. doi:10.3390/cli6010008.

[13] Hassan, W. H., & Hashim, F. S. (2020). The effect of climate change on the maximum temperature in Southwest Iraq using HadCM3 and CanESM2 modelling. SN Applied Sciences, 2(9), 1494. doi:10.1007/s42452-020-03302-z.

[14] Usta, D. F. B., Teymouri, M., Chatterjee, U., & Koley, B. (2022). Temperature projections over Iran during the twenty-first century using CMIP5 models. Modeling Earth Systems and Environment, 8(1), 749–760. doi:10.1007/s40808-021-01115-6.

[15] Afshar, M. H., Şorman, A. Ü., Tosunoğlu, F., Bulut, B., Yilmaz, M. T., & Danandeh Mehr, A. (2020). Climate change impact assessment on mild and extreme drought events using copulas over Ankara, Turkey. Theoretical and Applied Climatology, 141(3–4), 1045–1055. doi:10.1007/s00704-020-03257-6.

[16] Wilby, R. L. (1999). The weather generation game: A review of stochastic weather models. Progress in Physical Geography, 23(3), 329–357. doi:10.1177/030913339902300302.

[17] Hamidi Machekposhti, K., Sedghi, H., Telvari, A., & Babazadeh, H. (2018). Modeling Climate Variables of Rivers Basin using Time Series Analysis (Case Study: Karkheh River Basin at Iran). Civil Engineering Journal, 4(1), 78. doi:10.28991/cej-030970.

[18] Vallam, P., & Qin, X. S. (2018). Projecting future precipitation and temperature at sites with diverse climate through multiple statistical downscaling schemes. Theoretical and Applied Climatology, 134(1–2), 669–688. doi:10.1007/s00704-017-2299-y.

[19] Beecham, S., Rashid, M., & Chowdhury, R. K. (2014). Statistical downscaling of multi-site daily rainfall in a South Australian catchment using a Generalized Linear Model. International Journal of Climatology, 34(14), 3654–3670. doi:10.1002/joc.3933.

[20] Birara, H., Pandey, R. P., & Mishra, S. K. (2020). Projections of future rainfall and temperature using statistical downscaling techniques in Tana Basin, Ethiopia. Sustainable Water Resources Management, 6(5), 77. doi:10.1007/s40899-020-00436-1.

[21] Osman, Y., Al-Ansari, N., Abdellatif, M., Aljawad, S. B., & Knutsson, S. (2014). Expected Future Precipitation in Central Iraq Using LARS-WG Stochastic Weather Generator. Engineering, 06(13), 948–959. doi:10.4236/eng.2014.613086.

[22] Saddique, N., Bernhofer, C., Kronenberg, R., & Usman, M. (2019). Downscaling of CMIP5 Models Output by Using Statistical Models in a Data Scarce Mountain Environment (Mangla Dam Watershed), Northern Pakistan. Asia-Pacific Journal of Atmospheric Sciences, 55(4), 719–735. doi:10.1007/s13143-019-00111-2.

[23] Whitehead, P. G., Barbour, E., Futter, M. N., Sarkar, S., Rodda, H., Caesar, J., Butterfield, D., Jin, L., Sinha, R., Nicholls, R., & Salehin, M. (2015). Impacts of climate change and socio-economic scenarios on flow and water quality of the Ganges, Brahmaputra and Meghna (GBM) river systems: Low flow and flood statistics. Environmental Science: Processes and Impacts, 17(6), 1057–1069. doi:10.1039/c4em00619d.

[24] Haitham, L., & Al-Mukhtar, M. (2022). Assessment of Future Climate Change Impacts on Water Resources of Khabour River Catchment, North of Iraq. Engineering and Technology Journal, 40(5), 695–709. doi:10.30684/etj.v40i5.1925.

[25] Munawar, S., Rahman, G., Moazzam, M. F. U., Miandad, M., Ullah, K., Al-Ansari, N., & Linh, N. T. T. (2022). Future Climate Projections Using SDSM and LARS-WG Downscaling Methods for CMIP5 GCMs over the Transboundary Jhelum River Basin of the Himalayas Region. Atmosphere, 13(6), 898. doi:10.3390/atmos13060898.

[26] Semenov, M. A., Senapati, N., Coleman, K., & Collins, A. L. (2024). A dataset of CMIP6-based climate scenarios for climate change impact assessment in Great Britain. Data in Brief, 55. doi:10.1016/j.dib.2024.110709.

[27] Shahi, S., Hosseini, K., & Mousavi, S. F. (2024). Assessing the Effects of Climate Change on Temperature and Precipitation using CMIP6 models (case study: Damghan, Iran). Journal of Hydraulic and Water Engineering, 1(2), 163-177.

[28] Nouri, L., Mahtabi, G., Hosseini, S. H., & Prasad, C. V. S. R. (2024). Hydrological responses to future climate change in semi-arid region of Iran (Golabar and Taham Basins, Zanjan Province). Results in Engineering, 21. doi:10.1016/j.rineng.2024.101871.

[29] Muhaisen, N., Khayyun, T., & Al-Mukhtar, M. (2024). Drought forecasting model for future climate change effects in a regional catchment area in northern Iraq. Engineering and Technology Journal, 42(05), 1–15. doi:10.30684/etj.2024.144458.1634.

[30] Al-Hasani, B., Abdellatif, M., Carnacina, I., Harris, C., Al-Quraishi, A., Maaroof, B. F., & Zubaidi, S. L. (2024). Integrated geospatial approach for adaptive rainwater harvesting site. Stochastic Environmental Research and Risk Assessment, 38, 1009–1033.

[31] Saeed, F. H., Al-Khafaji, M. S., & Al-Faraj, F. (2022). Hydrologic response of arid and semi-arid river basins in Iraq under a changing climate. Journal of Water and Climate Change, 13(3), 1225–1240. doi:10.2166/wcc.2022.418.

[32] Semenov, M. A., Brooks, R. J., Barrow, E. M., & Richardson, C. W. (1998). Comparison of the WGEN and LARS-WG stochastic weather generators for diverse climates. Climate Research, 10(2), 95–107. doi:10.3354/cr010095.

[33] Hassan, W. H., Nile, B. K., Kadhim, Z. K., Mahdi, K., Riksen, M., & Thiab, R. F. (2023). Trends, forecasting and adaptation strategies of climate change in the middle and west regions of Iraq. SN Applied Sciences, 5(12), 312. doi:10.1007/s42452-023-05544-z.

[34] Semenov, M. A., & Barrow, E. M. (1997). Use of a stochastic weather generator in the development of climate change scenarios. Climatic Change, 35(4), 397–414. doi:10.1023/A:1005342632279.

[35] Muhaisen, N. Kh., Khayyun, T. Sh., Al Mukhtar, M., & Hassan, W. H. (2024). Forecasting changes in precipitation and temperatures of a regional watershed in Northern Iraq using LARS-WG model. Open Engineering, 14(1), 20220567. doi:10.1515/eng-2022-0567.

[36] Al-Maliki, L. A., Al-Mamoori, S. K., Al-Ansari, N., El-Tawel, K., & Comair, F. G. (2022). Climate change impact on water resources of Iraq (a review of literature). IOP Conference Series: Earth and Environmental Science, 1120(1), 012025. doi:10.1088/1755-1315/1120/1/012025.